Modeling an extreme dust deposition event to the French alpine seasonal snowpack in April 2018: Meteorological context and predictions of dust deposition

Foteini Baladima, Jennie L. Thomas, Didier Voisin, Marie Dumont, Clementine Junquas, Rajesh Kumar, Christophe Lavaysse, Louis Marelle, Mark Parrington, Johannes Flemming

Modeling an extreme dust deposition event to the French alpine seasonal snowpack in April 2018: Meteorological context and predictions of dust deposition

Foteini Baladima[1], Jennie L. Thomas[1], Didier Voisin[1], Marie Dumont[2], Clementine Junquas[1], Rajesh Kumar[4], Christophe Lavaysse[1,5], Louis Marelle[3], Mark Parrington[6], Johannes Flemming[6]

[1]Univ. Grenoble Alpes ,CNRS, IRD, Grenoble INP, IGE, 38000 Grenoble, France
[2]Univ. Grenoble Alpes, Université de Toulouse, Météo-France, CNRS, CNRM, Centre d'Etudes de la Neige, 38000 Grenoble, France
[3]LATMOS/IPSL, Sorbonne Université, UVSQ, CNRS, Paris, France
[4]National Center for Atmospheric Research, Boulder, CO, USA
[5]European Commission, Joint Research Centre, 21027 Ispra, Italy
[6]European Centre for Medium-Range Weather Forecasts (ECMWF), Reading, UK

Key Points:

- An extreme dust deposition event occurred in April 2018, that is in the top 95% of dust events to the Alps during the snow season.
- Wet (∼80%) and dry dust deposition (∼20%) contribute to total; dry deposition increases up to ∼1700m (∼40%) in the western part of the French Alps.
- Differences in dust deposition when increasing the model resolution are co-located with regions with improved predictions of precipitation.

Corresponding author: Foteini Baladima, foteini.baladima@univ-grenoble-alpes.fr

Corresponding author: Jennie L. Thomas, jennie.thomas@univ-grenoble-alpes.fr

Abstract

Mineral dust is an important aerosol in the atmosphere and is known to reduce snow albedo upon deposition. Model predictions of dust deposition events in snow covered mountain regions are challenging due to the complexity of aerosol-cloud interactions and the specifics of mountain meteorological systems. We use a case study of dust deposition between 30 March and 5 April 2018 to the French alpine snowpack to study the processes that control dust deposition to the seasonal snowpack. To understand processes controlling dust transport and deposition to snow we use a combination of *in situ* observations at Col du Lautaret in the French Alps, satellite remote sensing, the Copernicus Atmosphere Monitoring Service (CAMS) reanalysis global atmospheric composition, and the regional model WRF-Chem. Specifically, we investigate the role of increased model spatial resolution within WRF-chem in capturing mountain meteorology, precipitation, and predicted dust deposition. Regional model results are also compared to the reanalysis global CAMS products including aerosols in the atmosphere and predicted dust deposition fluxes. We conclude that predicted mountain meteorology (e.g. precipitation) is better with increased model resolution (3 x 3 km resolution WRF-Chem domain). This improved meteorology has significant impacts on predicted dry and wet dust deposition to the alpine snowpack. Dry deposition is important in the western part of the French Alps at low altitudes, while wet deposition dominates over the complex higher altitude mountain terrain.

1 Introduction

Mineral dust deposition to snow, including seasonal mountain snowpacks, can accelerate snow melting by causing a reduction in snow albedo (Painter et al., 2007, 2012, 2013; Reynolds et al., 2014; Tuzet et al., 2017; Skiles et al., 2018; Di Mauro et al., 2019). This reduction in snow albedo, referred to as snow darkening, triggers the well known snow albedo feedback mechanism in which reduced snow albedo accelerates the growth of snow grains, which further increases radiation that is absorbed and promotes snow/ice melt (Warren & Wiscombe, 1980; M. G. Flanner et al., 2007; M. Flanner et al., 2012; Hansen & Nazarenko, 2004; Tuzet et al., 2020). While dust impacts on the snow life cycle are clearly evident, accurate predictions of dust deposition in snow within mountain regions remains a challenge (Deems et al., 2013; Hock et al., 2019; Rahimi et al., 2020). This is due to a number of complex processes that contribute to accurate predictions of dust deposition starting with dust emissions, followed by transport/processing in the atmosphere within weather systems, and eventual deposition to snow within the complex mountain meteorological situation (Goudie & Middleton, 2001; Kok et al., 2012; Mahowald et al., 2014). At present, the accuracy of dust deposition rates predicted by models can limit our ability to correctly assess the impacts of dust on snowpack evolution (Tuzet et al., 2017, 2020).

Dust deposition to the mountains has recently been at the forefront of research on high altitude snowpacks (Lau & Kim, 2018; Sarangi et al., 2020; Das et al., 2020; Kok et al., 2021; Usha et al., 2021). There are two main types of deposition that result in dust arriving on/in snow: wet and dry deposition. Wet deposition is very efficient for removing aerosols from the atmosphere and occurs when aerosols are first taken up into clouds or scavenged during precipitation and then deposited with falling rain/snow (Pruppacher & Klett, 1997). Therefore, uncertainties in wet removal within mountains can be correlated with the uncertainties in predicted precipitation within models (Huneeus et al., 2011; Stocker, 2014; Regayre et al., 2018). Accurate prediction of precipitation is a known challenge in mountain regions, where there are clearly interactions between mountain topography and the occurrence of orographic precipitation. Dry deposition is the other important process by which dust arrives on snow, which involves a combination of direct contact between dust plumes that are transported long distances in the low/mid troposphere, and can directly arrive at high altitude mountain snowpacks as well as gravitational settling of large particles farther aloft (Seinfeld & Pandis, 2016). Understand-

ing the interactions between dust transport and deposition within mesoscale weather systems and microscale mountain meteorological systems remains a challenge.

Before being deposited to snow, dust plays an important role in the atmosphere and has both direct and indirect radiative impacts (Hansen et al., 1997; Haywood & Boucher, 2000). Long range dust transport is inherently tied to mesoscale weather systems bringing air from Africa mainly westward and southward towards/across Atlantic by the Saharan Air Layer but also to Europe (Chiapello et al., 1997; Sodemann et al., 2006; Salvador et al., 2014; Prospero et al., 2021). Aerosols themselves also impact weather systems due to their role as cloud condensation nuclei (CCN) and ice nuclei (IN) and their indirect (secondary) impacts on clouds (formation, droplet size, cloud darkening). Aerosols are linked to precipitation via their role in modification of clouds. Dust can have a significant impact on the energy balance within the atmosphere via warming upon absorbing solar radiation, or via cooling by participating in light scattering and modification of clouds (Hansen et al., 1997; Haywood & Boucher, 2000). Models that include a full description of aerosol-cloud interactions are best adapted to fully understand the role of dust within the atmosphere.

Between 30 March and 5 April 2018 a strong dust deposition event was observed within the seasonal snowpack at Col du Lautaret in the French Alps. Snowpit measurements after 4 April 2018 show that this dust layer stayed on the top of the snowpack during the entire snowmelt period, with implications for snow albedo and snow melt for the rest of the snow season. Tuzet et al. (2020) showed using the Crocus snowpack model (Vionnet et al., 2012; Tuzet et al., 2017) that the combined impacts of all light absorbing impurities shortened the seasonal snow cover by 11 days at Col du Lautaret in 2018 (Tuzet et al., 2020). These observations provide the motivation for understanding the specific conditions that result in this dust deposition event and an evaluation of how models can best represent events of dust deposition to snow.

The present study aims to answer the following scientific questions, with a specific focus on this extreme dust event that occurred in late March/early April 2018:

1. What are the large scale atmospheric drivers for this event of dust deposition to snow?
2. Does high resolution modeling including aerosol-cloud interactions improve the representation of dust deposition to snow?
3. Is accurate representation of specific mountain meteorology important for predicting dust deposition?
4. Are both dry and wet deposition important scavenging mechanisms during this event?

In order to answer these questions, we use a combination of satellite remote sensing, *in situ* measurements, and modeling tools, including dedicated Weather Research and Forecasting model coupled with Chemistry (WRF-Chem) model (Grell et al., 2005; J. D. Fast et al., 2006) predictions of the complete dust lifecycle. First, we present the observations and model data as well as we describe a specific WRF-Chem configuration model run conducted as part of this study in Section 2. We then present our results and discussion in Section 3. We show dust concentrations measured in snow pits during the 2018 winter-spring season in the French Alps (Tuzet et al., 2019) (Sect. 3.1). We compare 2018 to the multi-year dust transport frequency detected by satellite in Sect. 3.2. For this specific extreme dust deposition event that occurred in early April 2018, the main meteorological context is presented (Sect. 3.3). We present an evaluation of the simulated dust transport by comparing with satellite data and the Copernicus Atmosphere Monitoring Service (CAMS) reanalysis in Sect. 3.4. In Sect. 3.5, an evaluation of the WRF-Chem model predicted meteorology is performed. Finally, In Sect. 3.6 the WRF-Chem

model predicted dust deposition is presented and compared with CAMS reanalysis (Inness et al., 2019) and observations. The summary and conclusions are presented in Sect. 4.

2 Data and Methods

2.1 Measurements at Col du Lautaret

Col du Lautaret is a high mountain pass located in the French Alps at 2058 m above sea level (ASL) latitude=45° 02' 29" N longitute=6° 24' 38" E. The location is shown in Figure 1a (magenta circle). A field campaign took place during the snow season 2017-2018 with the objective of quantifying the concentrations of light absorbing impurities (LAPs) in snow including dust, elemental carbon (EC) and refractory black carbon (rBC) along with physical and optical properties of snow that were measured weekly. A detailed description of them and their impacts on snow evolution are found in (Tuzet et al., 2019).

Meteorological measurements were collected for the winter season 2017-2018 using an Automated Weather Station (AWS). Temperature, shortwave and longwave incident radiation, wind speed, atmospheric pressure, and relative humidity were the recorded parameters (Tuzet et al., 2019).

2.2 Satellite observations of aerosols, clouds, and snow

2.2.1 MODIS

The Moderate Resolution Imaging Spectroradiometer (MODIS) is a passive sensor that is onboard both NASA Aqua and Terra satellites. We use two MODIS data products in this study: aerosol optical depth (AOD) and snow cover. MODIS provides AOD data based on two retrieval algorithms. The Dark-Target (DT) algorithm, which retrieves data over dark surfaces and includes ocean surfaces and over vegetated/dark-soiled land. The Deep Blue algorithm retrieves data over bright surfaces such as deserts. For our study we use a daily product that combines these algorithms, the Dark Target and Deep Blue Combined data product (Platnick et al., 2015) Collection 6.1 data (MYD08_D3). This product provides daily coverage over all cloud-free and snow-free surfaces. From this we use maps of AOD at 550 nm at 0.1 Degree (∼10 km) spatial resolution. We also use the MODIS fractional snow cover from the the daily L3 Global 500 m SIN Grid, Version 6 data (Riggs et al., 2015). This product is generated by using MODIS calibrated radiance data products, the geolocation products, and the cloud mask products. MODIS AOD data was downloaded from NASA Giovanni (`https://giovanni.gsfc.nasa.gov/giovanni/`) and snow cover data from National Snow & Ice Data Center (`https://nsidc.org/data/MOD10A1/versions/6`).

2.2.2 CALIOP

Cloud-Aerosol Lidar with Orthogonal Polarization (CALIOP) onboard Cloud-Aerosol Lidar and Infrared Pathfinder Satellite Observations (CALIPSO) provides high-resolution vertical profiles of aerosols and clouds through the daytime and night-time at two wavelengths, 532 nm and 1064 nm. Here we use version 4 (V4) level 2 (L2) vertical feature mask (VFM) data product. The VFM algorithm takes into account the estimated particle depolarization ratio, the total attenuated backscatter, as well as the aerosol geographic location, the underlying surface type and the observed aerosol altitude (Omar et al., 2009) and identifies and classifies cloud and aerosol layers. Further, upon being detected aerosols are classified by type into the following categories: dust, polluted continental, polluted dust, smoke, clean continental, and clean marine. CALIOP data was downloaded from `https://www-calipso.larc.nasa.gov/products/`.

2.3 Ground based PM10 measurements

We use PM10 (coarse particles with an aerodynamical diameter of 10 μm or less) measurements from surface sites in France, including mountain sites to evaluate model predictions of dust transport. Specifically we use measurements from the Atmo Auvergne-Rhône-Alpes air quality monitoring network. As part of this network PM10 concentrations were monitored using automated analyzers, in accordance with recommendations of EN 16450:2017. PM10 measurements for 15 sites in France (see Figure 1a, green dots) were downloaded from `https://www.atmo-auvergnerhonealpes.fr/`.

2.4 Reanalysis data

Reanalysis datasets are temporally, spatially, and physically consistent products that combine data from earth observing systems, including satellites and *in situ* measurements, with numerical model simulations (ECMWF, 2021).

2.4.1 ERA5

ERA5 reanalysis which is the most updated global meteorological reanalysis from ECMWF and the Copernicus Climate Change Service (C3S) (Hersbach et al., 2020). This new reanalysis replaces the ERA-Interim reanalysis and is based on the Integrated Forecasting System (IFS) Cy41r2. ERA5 benefits from developments that have been done in model physics, core dynamics and data assimilation in the last 10 years. It provides hourly data at 0.25° by 0.25° (which is approximately ∼27.6 km x ∼14.6 km near the French Alps) spatial horizontal resolutions and 137 levels spanning the surface of the Earth to 0.01 hPa.

2.4.2 CAMS

The CAMS reanalysis (Inness et al., 2019) is the latest global reanalysis data set of atmospheric composition produced by ECMWF, consisting of 3-dimensional time-consistent fields of aerosols, trace and greenhouse gases. CAMS uses the updated IFS and the associated aerosol module (IFS-AER) includes five types of aerosols including desert dust which is represented with three bins (0.03–0.55 μm, 0.55–0.9 μm, 0.9–20 μm). The different aerosol types are externally mixed and both dry and wet deposition processes are included. The dust emissions are computed dynamically following Ginoux et al. (2001) dust source formulation and by taking into account prognostic meteorological variables, vegetation cover, soil moisture, snow cover provided by the model and the MODIS-derived UV-visible component of the land surface albedo (Morcrette et al., 2009).

CAMS reanalysis assimilates AOD observation from MODIS Aqua/Terra Collection 6 (Benedetti et al., 2009; Levy et al., 2018) retrievals. The CAMS aerosol configuration including AOD assimilation is described in Benedetti et al. (2019), which is based on Benedetti and Fisher (2007) and Benedetti et al. (2009). It should be noted that the vertical profile of the aerosol mixing ratio is not modified by the assimilation (Benedetti et al., 2019). CAMS reanalysis data have a global horizontal resolution of 0.75°×0.75° (∼80 km) and 60 vertical levels. It covers a time period from 2003 to 2020 with a temporal resolution of 3-hours. CAMS provide AOD datasets of multiple wavelengths, AOD data at 550 nm are used in this study.

2.4.3 SAFRAN

Système d'Analyse Fournissant des Renseignements Atmosphériques à la Neige (SAFRAN) is a mesoscale atmospheric analysis system from Météo-France which provides reanalysis data of surface meteorological variables (Durand et al., 2009). The data are provided on a grid based on mountain regions with similar meteorological characteristics called

massifs where the variability of data is a function of elevation, aspect and slope. For each massif, SAFRAN provides each parameter every 300 m at elevations up to 3600 m. SAFRAN uses an optimal interpolation to assimilate available observations including temperature, humidity and wind speed. Daily measurements including accumulated precipitation and temperature of around 500 meteorological stations over the French Alps at altitudes between 200 and 2500 m are included.

2.5 Precipitation data products

2.5.1 GPM

Global Precipitation Measurement (GPM) is an international satellite mission initiated by the Japan Aerospace Exploration Agency (JAXA) and the United States National Aeronautics and Space Administration (NASA) (Huffman et al., 2019). It provides high quality next generation precipitation observations using an international constellation of satellites including research and operational microwave sensors at a temporal resolution of 3 hours and global coverage. The Integrated Multi-satellite Retrievals for GPM (IMERG) algorithms intercalibrate, merge, and interpolate all GPM constellation satellites microwave precipitation estimates, together with microwave - calibrated infrared (IR) satellite estimates, precipitation gauge analyses, and potentially other precipitation estimators. The latest released GPM data version 6 V06B at 0.1 Degree (which is approximately ∼11 km x ∼5.8 km near the French Alps) spatial resolution was used in this study. GPM data was downloaded from `https://gpm.nasa.gov/data/directory`.

2.5.2 Radar

Météo France provides a weather radar rainfall mosaic dataset with a spatial resolution of 1 km and a temporal resolution of 5 min which covers the whole metropolitan France. It is a network of 30 radars and the volume scan of each radar is processed every 5 min to provide a quantitative precipitation estimate (QPE) map. The estimated precipitation is obtained by composing the QPE maps creating a national radar product called PANTHERE (Projet Aramis Nouvelles Technologies en Hydrométéorologie Extension et REnouvellement). While most of the operational radars in this framework are C and S band, X-band Doppler polarimetric radars are operated over the southern Alps (Yu et al., 2018).

2.6 WRF-Chem model

The WRF-Chem (Grell et al., 2005; J. D. Fast et al., 2006) model is a fully online coupled model. It permits the simulations of emissions, transport, mixing and chemical transformation of trace gases and aerosols simultaneously with the meteorology. The model is based on the Advanced Research WRF (ARW) core, which handles the meteorology, physics and transport processes (Skamarock & Klemp, 2008). The aerosol and chemistry components are completely consistent with the modeled meteorology, using the same grid and transport systems and same physics schemes for subgrid-scale transport (Grell et al., 2005). In our study, aerosol feedbacks/effects are included through the interaction of cloud physics with the model predicted aerosols (Easter et al., 2004; J. D. Fast et al., 2006). Here we use the regional model WRF-Chem 4.1.0 including an explicit description of aerosol-cloud interactions in order to quantify the relationship between dust deposition and weather systems. We set up the model using 3 nests (Figure 2), which are run using one way nesting. The model (D01) was run to include dust emissions through to deposition, from 14 March 2018 to 4 April 2018. We exclude the first 10 days of model run for D01 from analysis and consider this period as the model spinup. D01 includes the region of dust emissions in the Sahara, D02 is a regional domain over Europe, and D03 is a high resolution domain to capture the features of mountain meteorology. The meteorological initial and boundary conditions are provided by ERA5 (0.25° horizon-

tal resolution and 6 h temporal intervals). Chemical initial and boundary conditions (boundary conditions only for D01) are provided from the CAM-Chem model (see `https://www2.acom.ucar.edu/wrf-chem/wrf-chem-tools-community`, (Buchholz et al., 2019)). WRF-Chem-D01 domain includes the Saharan dust emission region and no initial and boundary conditions are provided for dust. For D01, spectral nudging (Miguez-Macho et al., 2004) also using ERA5 is applied and updated every 6 hours above the planetary boundary layer (PBL) for winds and temperature. For computational efficiency while also preserving the dust transport pathway from D01 to D02 and D03, D02 and D03 are run for a shorter time period. For D02 the model was run from 28 March 2018 and for D03 it was run from 29 March 2018 (18:00 UTC) to 4 April 2018. For numerical stability, time off-centering for vertical sound waves (*epssm*) and or the vertically propagating acoustic modes (*damp*) options were applied to all domains. The specific model physical, chemical, and emissions options for each domain are summarized in Table 1.

The model was run using the 8 bin Model for Simulating Aerosol Interactions and Chemistry (MOSAIC) aerosol scheme (Zaveri et al., 2008) including aerosol-cloud interactions (Easter et al., 2004; J. Fast et al., 2014), including the updates described in (Marelle et al., 2017). We use this particular setup due to the advanced description of aerosol physics and interactions with clouds. Specifically, MOSAIC treats aerosol processes including nucleation, coagulation, condensation, and evaporation. Aerosol-cloud interactions are described by aerosols acting as cloud nuclei, via in cloud chemistry, and via within and below cloud wet scavenging. Interstitial (suspended in air or between cloud particles) and cloud-borne aerosol particles (suspended in cloud droplets) are treated explicitly. Modeled aerosols can be activated or re-suspended (in air) depending on saturation, particle size, and aerosol composition. MOSAIC uses a sectional approach to simulate the aerosol size distributions (0.039-0.078 μm, 0.078-0.156 μm, 0.156-0.312μm, 0.312-0.625 μm, 0.625-1.25 μm, 1.25-2.5 μm, 2.5-5.0 μm, 5.0-10.0 μm) of five inorganic ions (sulfate, ammonium, nitrate and sea salt in the form of chlorine and sodium) and three primary aerosol species (black carbon, dust, and organic matter). Modeled Black Carbon (BC) includes all emitted black carbon mass that is included in the aerosol mass within MOSAIC. All particles within the same size bin are assumed to be internally mixed so that all particles within a bin have the same chemical composition and interactions with liquid clouds within each model grid cell. Within MOSAiC the hygroscopicity and CCN activity nucleating ability of aerosols is a linear combination of their aerosol chemical composition and considers aerosols as internally mixed within each size bin. Examples of the mass fraction for each chemical component modeled within each size bins over the dust emissions region and over the Alps are shown in Figure S1. Aerosol dry deposition includes Brownian and turbulent diffusion as well as gravitational settling (Wesely, 1989). In-cloud and below-cloud precipitation scavenging is included within the prediction of wet deposition as described by Easter et al. (2004).

Dust emissions are calculated online using the Goddard Chemistry Aerosol Radiation and Transport (GOCART) emissions scheme (Ginoux et al., 2001) and have been modified here according to Shao et al. (2011) to be optimized for Saharan dust. The basic parameters of any dust emission model are the threshold friction velocity as well as the horizontal and vertical mass flux of dust as wind speed near the surface should be sufficient to lift surface particles and entrain them into the atmospheric boundary layer (Kok et al., 2012). GOCART scheme uses the simulated from WRF-Chem wind speed near the surface and calculates online dust emissions. We also modified the model to save dust deposition rates for each aerosol size bin within MOSAIC.

3 Results and discussion

3.1 Observed dust deposition to snow in winter/spring 2018

Dust deposition to snow at Col du Lautaret in the French Alps (Figure 1a, magenta circle) was measured within snow pits during the 2018 snow season (Figure 1b), measurements described in Tuzet et al. (2019). Specifically, a large dust deposition event was measured in the snow pit conducted on 4 April 2018 (Figure 1b, dark red layer) that was buried slightly below the surface. Given the earlier snow pit that was completed on 13 March 2018 did not contain this layer with enhanced dust concentrations, we can clearly identify this dust deposition occurred between 13 March and 4 April 2018 (as already noted in Tuzet et al. (2019)), the time period is shown by a gray box in Figure 1b. We show the regional extent of snow cover during the same time period on 22 March 2018 in Figure 1a to depict the regional extent of alpine snow cover during the deposition event. The simulated snow cover extent during the deposition event from WRF-Chem D02 is shown in Figure S2a).

3.2 Multi-year analysis of dust transport during the alpine snow season

In this section we aim to understand how this observed dust deposition event fits into the multi-year context of dust transport during the winter season. For this, we use satellite observations of AOD from MODIS Aqua and reanalysis values of AOD from CAMS using all data available from 2002 to 2021. The availability of MODIS AOD retrievals over snow covered areas is significantly limited by high albedo as well as by the frequent occurrence of cloud cover (see Supplement, Figure S2b). To overcome this limitation, we use a larger region than the snow covered Alps (2.5 °E, 38.5 °N, 11.5 °E, 48.5 °N, region shown in inset of Figure 3) to identify dust transport events. We calculate the average AOD within this region as a daily average shown in Figure 2. The highest average AOD values that lie above the 95^{th} percentile (teal points) and above the 99^{th} percentile (magenta points) thresholds for AOD values for the snow season (noted in gray, December to April) are shown. We classify consecutive days with enhanced AOD as the same dust transport event. The red cross shows our specific dust transport event that occurred in early April 2018. This analysis allows us to characterize this as extreme event due to the fact that it is among the top 5 percentile of all dust transport events during snow season between 2002-2021. Looking at AOD MODIS retrievals from 13 March to 4 April (data not shown), we identified that this dust transport event occurred between 31 March 2018 and 3 April 2018. We show the AOD MODIS retrievals for the key period in Sect. 3.4.

3.3 Mesoscale meteorological conditions in this dust deposition event

AOD from MODIS and CAMS shown in the prior section provided the specific time window when this dust transport event occurred, between 31 March 2018 and 3 April 2018. In this section we show the prevailing atmospheric circulation patterns that dominate during this dust transport event that results in deposition to snow. The days before and during the dust outbreak are impacted by the negative North Atlantic Oscillation (NAO) phase (Meteo France, 2021). When NAO is negative, both sub-polar low and subtropical high are weaker than average, the Atlantic Jet Stream has a more zonal (west-to-east) orientation which results in a convergence of winter Atlantic storms in central west Europe.

The synoptic conditions of the dust event are described using the ERA5 reanalysis. In Figure 4a we show the 700 hPa geopotential height at 12:00 UTC from ERA5 on each of the days of the event. On 1 April 2018 (Day-2) a ridge extended over north central Africa while a trough extended from east Europe to the Mediterranean sea (Fig-

ure 4a). On 2 (Day-1) and 3 (Day 0) of April the ridge axis moves eastwards causing south-westerly flow, over the Mediterranean sea towards the French Alps, with high wind speeds (up to 10 m/s at sea level in Figure S3a and 20 m/s at 700 hPa height Figure 4a). At the surface, a high-pressure system centered between Sicily and center-north Africa extends up to Algeria while a thermal low pressure system extends over north Africa including Morocco (see supplement Figure S3a Day-1 and Day-2). Additionally, a low pressure system (Atlantic low) is displaced towards northwest of Spain. Large amount of water vapor is transported in the Alps (see supplemental Figure S3b) and precipitation events are expected in the region. All of these factors result in a dust enriched air mass that is transported from the Sahara and arrives at Col du Lautaret with this weather system on 3 April 2018.

We compare WRF-Chem D01 with ERA5 geopotential height at 700 hPa to evaluate the model ability to reproduce the meteorology that drives this event (Figure 4). WRF-Chem D01 captures well the general circulation during all the days of the event. The model is able to represent the timing and the horizontal extent of both ridges and troughs. The strength of the simulated Saharan high is slightly overestimated compared to ERA5 reanalysis data (on average $\sim$50 m) during the event. Major differences between ERA5 and WRF-Chem D01 occur on 31 March (Day-3) when the model shows stronger wind speed and higher geopotential height at 700 hPa.

3.4 Evaluation of modeled dust transport

The AOD simulated by WRF-Chem (D01) over the dust source region and during long range transport are compared to MODIS Aqua AOD and CAMS AOD in Figure 5. On the 30 and 31 March the dust plume extends over Algeria and Tunisia and on 31 March dust is clearly transported into the region of southern Italy and Sicily including the central Mediterranean Sea. The spatial distribution of the predicted AOD from both WRF-Chem and CAMS are in a good agreement with the satellite measurements. On 2 and 3 April the dust plume shifted west and moved to the southern part of France and southeast Spain. The lack of satellite AOD retrievals over France and the Alps is due to cloud coverage and/or the presence of high albedo snow, limiting a direct comparison between MODIS and the models as the dust plume arrives further north on 2-4 April.

Comparing the models with the observed AOD values, we note that CAMS agrees well with AOD, while WRF-Chem tends to over-predict AOD in the dust emissions source regions (by ~ 0.15). We note that AOD is assimilated into the CAMS reanalysis (Benedetti et al., 2009; Levy et al., 2018) and a very good agreement is therefore expected. There is no assimilation of AOD or aerosol in WRF-Chem. As a result, no correction is applied to the over-prediction of the intensity of the plume, which is clearly over Africa, where WRF-Chem predicts high AOD values over a larger spatial extent than detected by MODIS. We have specifically used the parameters for the Saharan dust within the GOCART dust emissions scheme within WRF-Chem according to Shao et al. (2011). Upon adjusting these parameters, the total dust emission are reduced and lower AOD is predicted compared to the standard version of the model (see supplemental Figure S4). However, a general over prediction of winds by WRF-Chem at the surface in Africa compared to ERA5 (see supplement, Figure S5) is the likely cause of the enhanced AOD values compared to MODIS. The simulated dust concentrations vary due to the differences in the treatment of aerosols and differences in simulated meteorology. In addition, CAMS includes assimilation of satellite derived aerosol AOD, while WRF-Chem does not include any assimilation. Both CAMS and WRF-Chem use similar dust emission schemes. The dust emission fluxes, which result in these atmospheric concentrations also differ due to differences in simulated surface meteorology (atmospheric stability and surface wind speed), surface properties (such as soil particle size distribution, surface roughness and soil moisture) as well as the models resolutions. For example, the spatial resolution of soil mois-

ture and vegetation cover can affect the estimated values of AOD and the dust storm spatial distribution.

To understand if this general over estimation of dust emissions impacts our WRF-Chem model prediction, we have completed FLEXPART-WRF potential emissions sensitivity (back trajectory) analysis (see supplement, Figure S6). This shows that the main dust emission source region for air that arrives at Col du Lautaret on 3 and 4 April 2018 was in the very northern portion of Africa, where WRF-Chem predicted dust is in better agreement with the MODIS AOD values than the largest portion of this dust storm farther south.

The vertical distribution of dust in the atmosphere is important for the residence time of the dust particles and their atmospheric transport pathways. The atmospheric lifetime and transport distance for dust particles increases when it is lifted and transported higher in the atmosphere. On Figure 6 we compare aerosols within the atmosphere detected by CALIOP (aerosol detection and aerosol sub-type) for the CALIPSO overpasses shown in black on Figure 6. We show the four overpasses that capture this dust transport event: one on 31 March, one on 3 April, and two on 4 April. For this, we extract the total concentration of dust from the CAMS results (all dust bins) and WRF-Chem model (other inorganic aerosols, which are primarily dust using D01) along the CALIPSO overpass and provide a vertical profile along each overpass. We show that the aerosol retrievals from CALIOP are limited by the location of high altitude clouds above 8 km for some overpasses. These include: 10-15 deg Lat (Figure 6a), 35-45 deg Lat (Figure 6c), and 40-50 deg Lat (Figure 6d). Clouds limit the ability to directly detect the main portion of the dust transport event during deposition to snow over the Alps, on 4 April. However, we can still evaluate the representation of dust farther south and prior to being transported into the region. The aerosol layer detected by CALIOP (orange color, Figure 6 panels (a-d) for all CALIPSO overpasses is mainly identified as dust (yellow color, Figure 6 panels (e-h)) by the VFM mask algorithm.

First, we look how the models represent dust near the source region on 31 March and 2 April 2018. On 31 March (Figure 6, first column) the dust layer extends up to 6 km altitude and as far north as 33°N in the satellite retrievals and in both models outputs. Satellite measurements between 10°N and 17°N are missing due to cloud attenuation. On 2 April (Figure 6, second column) the dust layer was lifted higher in the mid troposphere up to 7 km according to CALIOP. The WRF-Chem model captures the depth of the dust layer for this overpass, but the simulated dust plume peak is shifted further north compared to the measured satellite retrievals. However, the CAMS dust layer between 5°N and 20°N is lifted higher in the atmosphere than detected by CALIOP.

We now look at dust as it arrived over Europe and the region of the Alps, we look at the overpasses on 4 April 2018, which is during the deposition event. Both CALIPSO overpasses on this day (Figure 6 (g) & (h)) show there are thick clouds in the mid-troposphere at latitudes spanning from 40°N to 50°N. For these latitudes the signal is attenuated and we cannot compare the horizontal and vertical distribution of the dust plume over the Alps. Both models show that a significant dust plume is transported to the region of the Alps on 4 April. However, the vertical distribution of the modeled plumes for both overpasses are represented differently in WRF-Chem and CAMS. In general, WRF-Chem has a smaller vertical extent of the plume with a more concentrated dust layer near the surface, which is in agreement with CALIOP. CAMS predicts a dust layer that extends higher into the atmosphere, which is in less good agreement with the CALIOP retrievals. The vertical extent of the dust plume plays a key role for the dust particles lifetime and transport. The lifetime of dust particles within the PBL is relatively short due to turbulent mixing. Dust particles in the free troposphere have a longer transport distance due to their longer lifetime and they can later be entrained into the local mixed layer i.e through the cloud-top by cloud-induced mixing. While the exact connection between the vertical extent of the plume and deposition rates over the Alps is not well quantified, we note

that ensuring accurate vertical distribution and co-location with clouds is important for wet removal, while accurate dust concentrations near the ground are clearly important for accurate prediction of dry deposition.

In Figure 7, we compare WRF-Chem (blue line) and CAMS (green line) aerosol predictions to 15 ground based air quality monitoring station (black line) to evaluate if the model captures correctly dust that is transported to the region of the French Alps during this event. We show a comparison between WRF-Chem (D01) and CAMS (3-hourly data) predicted PM10 and the Atmo Auvergne-Rhône-Alpes air quality observations, which include three types of measurement sites (urban, semi-urban, and background), in Figure 7. For this we use modeled predicted surface value (lowest model level) and interpolate the results to the latitude and longitude of each measurement site. We use all three types of measurements sites that are part of this air quality network for our evaluation. The exact timing of the arrival of this dust storm in the French Alps is noted in the gray background on all panels.

Both models in general capture the scale of PM10 before and during the event. CAMS predicts PM10 values though shows a bias more pronounced than WRF-Chem D01 values when compared to observations over the whole time period. This bias is often caused by an increased night-time bias and can be correlated with the strong diurnal cycle which is more pronounced in CAMS. The PBL height and evolution impacts the PM10 measurements but the key mechanisms may vary at the different altitudes and sites. Surface dust concentrations from both models and observations causes surface PM10 to increase significantly during the event in all measurements sites across the French Alps. This increase shows that air pollution in the region can be caused by non local sources. However, we note that the urban and semi-urban sites (such as Chamonix and Demi-Quartier) do not agree as well with the WRF-Chem outside the times of this specific dust event. Moreover we note that both models overestimate surface PM10 during the event at some measurement sites (such as Ordonnaz, Bourg en Bresse, Saint-Germain-Sur-Rhone). This reveals that the predicted dust plume from both models has higher dust concentrations compared to the observations closer to the surface.

We show that both timing and quantity of dust transport to these sites, which are located at a variety of altitudes (from 125 to 1243 m ASL) is correctly represented by WRF-Chem. This evidence provides us confidence that within WRF-Chem dust within the atmosphere can be used for accurate predictions of dust deposition to snow in the region of the the Alps.

3.5 Evaluation of WRF-Chem predicted mountain meteorology and precipitation

3.5.1 Predicted regional scale precipitation and temperature

In this section, we evaluate regional scale predicted WRF-Chem meteorology using GPM satellite precipitation data, ground based Météo France Radar rainfall product, SAFRAN reanalysis data and ground station measurements. First, we look at the influence of model resolution on predicted precipitation in order to understand how differences in precipitation rates may be impacted model predictions of wet deposition of dust.

The spatial distribution of daily precipitation rates simulated by WRF-Chem, and observed by GPM and the Météo France Radar product is illustrated on Figure 8. The rain rates are qualitatively well reproduced by the model as well as the spatial variability of the daily values. WRF-Chem D02 predicts higher precipitation rates than D01, which are mainly driven by the differences in the spatial resolution of the topography.

On 4 April (see Figure 8, last row) during the deposition event, WRF-Chem D03 underestimates precipitation over the Alps compared to both GPM and Radar products, while using a convection permitting configuration (cumulus scheme deactivated) at this resolution (3 km × 3 km horizontal resolution). These values are also lower than WRF-Chem D01 and D02 resolution predictions, where this precipitation event is produced by convective precipitation. We note that WRF-Chem D03 should be able to explicitly reproduce convection processes and associated precipitation through the description of the cloud micro-physical processes (see Table 1). Therefore, in our base run there is no convective parameterization activated in D03. To check if including parameterized convection in D03 improves the predictions of precipitation on 4 April we have completed a sensitivity run with a convective parameterization activated for this day (results in Figure S7). When activated, the model uses both the cumulus scheme and microphysics to produce precipitation. This increases the daily simulated precipitation over the western mountain sides while decreases the simulated precipitation in the center and north east part of the Alps. Figure S7 illustrates the convective and non convective daily precipitation during this day as well the differences of total precipitation between the two runs. The relatively high amount of convective precipitation implies that mainly the scale of convective patterns on the western side of the Alps is smaller than 3 km and the model is not able to explicitly reproduce them through microphysical processes.

The total predicted mean daily precipitation during the event at D01, D02 and D03 resolutions as well as their differences are presented on Figure 9b and 9d. Figure 9a shows the topography over the French Alps at the 3 different resolutions. The main differences between them (Figure 9c) are depicted at the summits and ridges up to 1200 m as well as valleys. Differences in topography can alter surface moisture and consequently can influence precipitation patterns. Topographic features may stay unresolved while smoothed topography can enhance vapor transport to high elevations, increase available moisture and reduce stability. Increasing the resolution, the distribution of precipitation follows the higher topographical representation of the Alps (Figure 9b), revealing the importance of the accurate topography representation when simulating orographic precipitation. The relationship between the elevation differences and precipitation during the event when increasing the resolution shows an increase in precipitation related to the representation of orography (see supplement, Figure S8) . Specifically, the differences maps (Figure 9d) show higher precipitation rates over mountain peaks and dryer valleys when increasing the resolution.

SAFRAN data provides wide spatial coverage (French Alps) with high accuracy at different altitudes (Durand et al., 2009). The accurate representation of the spatial distribution of precipitation is crucial for a reliable estimation of wet deposition at different elevations over the French Alps. In order to overcome the spatial inconsistencies caused by the different grid representation of WRF-Chem outputs and SAFRAN reanalysis product, WRF-Chem data have been adjusted to SAFRAN semi-distributed grids/massifs. Figure 10 shows the spatial distribution of the co-located SAFRAN and WRF-Chem D01, D02, D03 mean temperature (at 2 m) Figure 10a) and precipitation (Figure 10b) during the 30 March and 3 April event at different altitudes.

A systematic cold bias is shown in the simulated mean 2 m air temperature by all model resolutions D01, D02, D03 and at all altitudes (Figure 10a). This bias has a high dependence on model resolution. By increasing the resolution the cold bias is moderated up to 2100 m altitude. We note that even massifs with significant mis-represented altitudes by the WRF-Chem topography have large temperature cold biases. This is a quite well known WRF problem and several studies have underlined it (Kumar et al., 2012; Jiménez & Dudhia, 2013; García-Díez et al., 2013; Karki et al., 2017; Meng et al., 2018). The spatial distribution and magnitude of precipitation is in general well captured by the model at the different altitudes (Figure 10b). Specifically, at low altitudes (below 1200 m) the simulated values from WRF-Chem are in a good agreement with SAFRAN

reanalysis data. At higher altitudes the model overestimates mean precipitation in the southern region and underestimates it in the north-west region of the French Alps compared to SAFRAN reanalysis. This bias is more pronounced for D03 and can be correlated with the pronounced cold bias in the simulated surface temperature at these altitudes. On 4 April WRF-Chem D03 resolution predicts only high altitude precipitation (above 2100 m) and underestimated mean precipitation in the lower altitudes when compared to SAFRAN (see supplement, Figure S10b).

3.5.2 Col du Lautaret

A comparison of the *in situ* observations at Col du Lautaret and the simulated values by WRF-Chem D01, D02, D03 of temperature, wind speed, specific humidity and precipitation is shown in Figure 11. It should be noted that the difference of the actual elevation of the measurement station and of the model grid cell station elevation is 191 m (D01), and 176 m (D02), 78 m (D03). A bias correction has not been applied as the aim of this work is to highlight the impact of the different model resolution to the predicted meteorology relevant to dust deposition events over complex terrain.

Figure 11a shows the time series of the hourly 2 m simulated temperature from WRF-Chem and 3.53 m from the ground observed temperature at Col du Lautaret during the simulated period. The diurnal cycle is well represented by the model. Temperature simulated from WRF-Chem D03 is in close agreement with measured values than WRF-Chem D01 and D02 between 30 March and 2 April, confirmed by RMSE values (see supplement Figure S11a). D01 and D02 are mainly underestimating the 2 m temperature by up to 6 K and 5 K respectively. D03 overestimates the 2 m temperature during the dust deposition event (light gray shaded area in Figure 11); during this period D01 and D02 are in a better agreement with the observations.

The accurate representation of precipitation is crucial for the calculation of wet removal of aerosol such as dust. The observed values have been derived from snow height measurements. The daily values are shown in Figure 11b. The precipitation events during the simulated period are in general underestimated in comparison to observations of the main snow event that contributed to dust deposition on 3-4 April. It should be noted that there is a shift on the timing of the precipitation that occurred on 1 April (12 hours) while the timing of the precipitation event between 4 and 5 April is accurately captured by the model. Precipitation events can be local phenomena and may be produced by convective rain, therefore our WRF-Chem D03 resolution of 3 km cannot fully reproduce them.

Wind speed at 10 m has an important effect on the horizontal transport of air masses. The underestimation or overestimation of wind speeds can lead to a misrepresentation of dry or/and wet deposition flux. We should underline that the wind speed measurements of the weather station at Col du Lautaret are at 5.18 m from the ground and are compared with the 10 m wind speed from the model. This can cause systematic biases between the measurements and the simulated values. Figure 11c shows an overestimation in mean wind speed more pronounced for D01 and D02 than D03 caused by the overestimation of the maximum wind speed values (see also boxplot supplement, Figure S11b). Specific humidity time-series during the simulated period are shown in Figure 11d. The model is in general in a good agreement with observed values during the simulated period.

In summary WRF-Chem model captures well the temporal evolution of the meteorological conditions during the dust event. The simulated mountain meteorology from WRF-Chem highest resolution D03 shows in general a better agreement with observations compared to WRF-Chem D01 and D02 spatial resolutions. The synoptic circulation is well represented from WRF-Chem, the horizontal resolution of 3 km is not enough though to resolve all the relevant topographic features over complex terrain. Wind speed,

temperature and precipitation can alter wet and dry deposition rates over the Alps via the interaction of regional atmospheric circulation and mountain boundary layer dynamics. A study that quantifies the advection and entrainment of free tropospheric air enriched with dust aerosols during the boundary layer development is needed.

3.6 Predicted dust deposition

In this section we show the predicted total wet and dry deposition from WRF-Chem (at different resolutions) and CAMS and compare this with estimates derived from correcting model predicted dust deposited rates from the ALADIN model (as described in Tuzet et al. (2019)) that were adjusted to correctly predict the dust concentrations measurements in snow pits (from here on, we refer to these data as *observations*).

We also investigate the influence of terrain resolution topographical features both on wet and dry deposition processes. In the previous sections we discussed the representation of dust within the atmosphere in both WRF-Chem and CAMS and precipitation rates over the Alps from WRF-Chem. Here, we look at how dust transport, mountain specific terrain, as well as weather/local scale meteorological processes impact predicted dust deposition rates.

First, we focus on understanding simulations of dust deposition locally at the Col du Lautaret site. Figure 12 compares hourly accumulated wet (Figure 12a) and dry (Figure 12b) dust deposition to snow at Col du Lautaret from WRF-Chem (D01, D02, D03) and CAMS with observations. The timing and magnitude of the simulated wet and dry deposition rates by WRF-Chem are in a good agreement with the observed values. There is no significant difference between the different model resolutions specifically at the Col du Lautaret site. There is a shift in the timing of the dust deposition event that is predicted by CAMS. The WRF-Chem model underestimates dust wet deposition by approximately a factor of 3.7 (D01), 3.9 (D02) and 2.9 (D03) compared to the observed accumulated value during the event. In contrast, CAMS underestimates this wet deposition value by a factor of $\sim$7.7. Dry deposition is underestimated from WRF-Chem by a factor of 4.5 (D01), 9.1 (D02), 3.9 (D03), and by a factor of 20.7 from CAMS. In summary, there is no clear improvement in WRF-Chem predicted dust deposition values specifically at Col du Lautaret upon increased model resolution, despite the improved regional meteorology (including precipitation) for D03 (see Section 3.5). The model predictions would require an even higher resolution than 3 km in order to represent the intersection of three different mountains at this site which are very close in proximity. However, all WRF-Chem domains are closer to the observed peak deposition values than the CAMS predictions.

Next, we look at the regional scale influence of WRF-Chem model resolution on dust deposition rates and compare them with CAMS and regional precipitation patterns and terrain characteristics in Figure 13. We show the total (first row) wet (second row) and dry (third row) accumulated deposition rates on 3 April 2018 at different model resolutions. In order to overcome the spatial inconsistency caused by the different horizontal resolutions WRF-Chem D01 and D02 simulated values have been regridded to D03 horizontal resolution.

The dust deposition rates simulated by WRF-Chem D01, D02, D03 show that the event includes both wet and dry deposition of dust with a larger contribution of wet deposition. Wet deposition dominates over the Alps, where we predict deposition rates over 10^3 mg m^{-2} in southern part of the French Alps. The higher differences between the different domains (D03-D01, D03-D02) are found to be co-located with the maximum differences in predicted precipitation (see supplement Figure S12). The total and wet deposition increases over the Alps and decreases over the Po valley located at the eastern part of the French Alps for the highest resolution domain (D03, 3×3 km resolution). We compare WRF-Chem lowest resolution (27×27 km resolution) model results with the CAMS

reanalysis product (D01-CAMS). The contribution of wet deposition to the total dust deposition rate predicted by CAMS is significant. Total and wet deposition rates from CAMS are lower by up to 3 orders of magnitude than the WRF-Chem D01 predicted values. Wet deposition is directly linked with cloud formation and precipitation and this bias is maybe caused and/or impacted by the CAMS representation of both wet removal in clouds and precipitation. To better understand this, we plot ERA5 accumulated precipitation and we show that is co-located with the accumulated wet deposition on 3 April 2018 (Supplement Figure S13). In summary, there are large differences in wet deposition predictions which implies that different parameters are governing the wet scavenging in different models and at different model resolutions (i.e vertical air mass fluxes, vertical distribution of precipitation, particle sizes). A study that separates the removal by convective and synoptic precipitation will give a better understanding of these differences.

The dry deposition rates are highest in the western part of the French Alps, where the dust plume is most present in the atmosphere (prior to rain out over the highest mountains in the Alps) and dust can deposit via either turbulent dry deposition (surface contact) or gravitational settling (dust deposition from aloft). The Saharan dust is transported over the Alps by a westerly flow and as a result dry deposition is most prominent on the western side of the massifs. The strongest impact of model resolution on dry deposition is an increase in dry deposition in the western Alps (following $\sim$ 1000 m contour interval) and a decrease in dry deposition for just east, where the terrain is above $\sim$1000 m (Figure 13). Dry deposition at the western Alps is the same order of magnitude as wet. Figure 14a shows the estimated (from WRF-Chem D03) altitude dependence of dry to total dust deposition at the western French Alps (longitude less than 6.5°E). The percentage of dry deposition increases with altitude from $\sim$800 m to $\sim$1700 m and decreases at higher altitudes, peaking at $\sim$1700 m. Dry deposition contributes $\sim$30% to $\sim$40% (mean values) up to $\sim$1700 m to the total dust deposition rates while it decreases up to less than 10% at higher altitudes above $\sim$1700 m. The PBL height over western Alps follows a similar distribution (increases) as dry deposition rates up to $\sim$1700 m (Figure 14b). Depending on the horizontal wind shear with respect to the altitude, Alpine sites can be within the PBL which contains dust enriched air mass, and favors dry dust deposition. CAMS predicts lower dry deposition rates (by up to 2 orders of magnitude) compared to WRF-Chem D01. These differences originate from differences in dry deposition velocities, model topography, as well as differences in vertical distribution of dust in atmosphere.

In summary, models resolutions play an important role in dust transport and deposition processes over the French Alps. Mountains specifically impact precipitation via orographic lifting of air masses that leads to conversion of the condensate to precipitable particles by a combination of smaller-scale convection, turbulent air motions, and cloud microphysics (Rotunno & Houze, 2007). High-resolution simulations treat the orographically forced precipitation in a more physically accurate way that is consistent with mountain terrain, which is essential for wet deposition. Moreover, the higher 3 km resolution domain (WRF-Chem D03) may represent more accurately the channelization of the dust flow through valleys (Bessagnet et al., 2017). The more accurate topography representation can alter the mountain-valley circulation and may block the simulated dust fronts, limiting the dust transport.

We show that the range of the simulated deposition fluxes from WRF-Chem and CAMS varies. To better understand and address the reasons for such differences, we show the spatial distribution of dust deposition fluxes (total, wet and dry) at each size bin over the French Alps, from both WRF-Chem and CAMS (Figure 15) on 3 April 2018. WRF-Chem deposition fluxes from the first 4 size bins (0.039-0.078 μm, 0.078-0.156 μm, 0.156-0.312μm, 0.312-0.625 μm) have been accumulated and presented here at one size bin (0.039-0.625 μm) (first column).

Over the Alps, the simulated deposition fluxes are strongly dominated by the coarse size bins i.e particles with diameters over 0.9μm for CAMS and 1.25 μm for WRF-Chem. However, CAMS exhibits a general underestimation of deposition fluxes (total, wet and dry) compared to WRF-Chem over the region at these size bins. The WRF-Chem deposition size bin scheme (MOSAIC) has 3 bins over this range (1.25-2.5 μm, 2.5-5.0 μm, 5.0-10.0 μm), where the gradient of deposition velocity is high, while CAMS has only one (0.9–20 μm). As a result, coarse dust particles from CAMS may be affected mainly by dry and/or wet deposition processes near the dust source area. Moreover, CAMS shows a more important contribution of fine dust particles (diameters less than 1 μm) to wet and total dust deposition over the Alps compared to WRF-Chem. This reveals that these differences may come from first, the variations of the simulated vertical mass flux of dust (saltation flux) from the surface and/or its distribution into the dust emission bins from CAMS and WRF-Chem schemes. Second, the different simulated vertical distribution and the particle size distribution within the atmosphere from WRF-Chem and CAMS affects dust transportation and deposition. Finally, CAMS assimilates AOD MODIS retrievals therefore modelled optical properties may shift towards observations even when the modelled microphysical properties differ. Finer particles exerts a larger effect on aerosol extinction coefficient per unit mass than coarse particles and may be fine-tuned to represent the observed optical depth.

In Figure 15(c) we show the simulated dust deposition (total, wet and dry) at all size bins from the highest (D03) WRF-Chem resolution. Model resolution has a strong impact on spatial distribution of dust deposition at all size bins, with more pronounced differences at dust deposition fluxes related to size bins with high dust deposition rates (above 0.625 μm). By increasing the resolution, the spatial distribution of dust deposition (total, wet and dry) is altered and more dust is deposited over the Alps following the higher representation of the topography (D03). It should be noted that the main size bins that contribute to the dust deposition remain the coarse size bins and is dominated by dust particles located between 2.5-5.0 μm and 5.0-10.0 μm. Dust distributions simulated from WRF-Chem are in agreement with dust measurements in snow/ice over the Alps (3-5 μm Wagenbach and Geis (1989); μm 3.2-8.5 μm Di Mauro et al. (2019))

In summary, both models capture the timing of the dust event, although the intensity is underestimated. Wet deposition is seen to be the dominant removal mechanism during this specific event, while the dry deposition can play an important role at particular low altitudes at the lee side of the massifs. Wet deposition contributes $\sim$79.5 % and dry deposition $\sim$20.5% to total simulated deposition rates from WRF-Chem D03 (wet deposition 84.5 % and dry deposition 15.5% at altitudes above 850 m). Dust coarse size bins dominate simulated deposition fluxes during this event from both CAMS and WRF-Chem model.

Model aerosols in the lowest and mid troposphere and aerosols scavenging processes within the models and model resolutions play an important role and drive the uncertainties and errors in the magnitude of wet deposition rates. A combination of factors should be taken into account when simulating and representing deposition rates over mountains i.e the French Alps. First, the magnitude and vertical extension of the dust plume that is transported into the mountain region is important both for wet and dry deposition. Second, mountain meteorology can alter aerosols scavenging by clouds. Third, the representation of aerosol cloud interactions (explicit treatment of aerosols as CCNs and INs) and scavenging processes changes in different models and model resolutions.

4 Summary and conclusions

In this paper, we focus on understanding the factors that control dust deposition to snow in the French Alps using a case study in April 2018 using satellite remote sens-

ing, modeling, and observations in the Alps. We first focus on understanding model predictions at regional scale and of mountain meteorological conditions.

Our study contributes to link local and regional scale processes which drive dust deposition in remote mountain regions. It provides a basis of understanding the processes and uncertainties on modeling dust deposition events over mountains at different resolutions. The effect of spatial resolution on model simulated mountain meteorology including precipitation is specifically explored. Our results show that the WRF-Chem model meteorology is very sensitive to model resolution, which is due to the improved representation of topography. Increasing the resolution the updraft wind speeds and the convective updraft areas changes and alters the simulated meteorology. A future ensemble study is needed to quantify these changes as a function of dust concentration and environmental conditions.

We also use remote sensing and ground based observations of aerosols (MODIS AOD, CALIOP retrievals, PM10 measurements) to evaluate both WRF-Chem and CAMS representation of this dust transport event. WRF-Chem model overestimates AOD and surface PM10 during the event while underestimates deposition fluxes compared to observations at Col du Lautaret. CAMS reanalysis assimilates MODIS AOD retrievals and a good agreement between MODIS and CAMS AOD is shown. CAMS overestimates the surface PM10 values and underestimates dust deposition fluxes compared to both observations and WRF-Chem D01 simulated values. The comparison of deposition rates between WRF-Chem D01 and CAMS shows a difference, mainly correlated to wet deposition, up to 3 orders of magnitude.

A combination of factors results in the underestimation of deposition fluxes at Col du Lautaret despite the overestimation of aerosol mixing ratio within the atmosphere compared to observations from both models. First the overestimation/underestimation of dry deposition velocity can overestimate/underestimate size bins concentrations of dust particles transported in the atmosphere. Moreover, biases and errors in the magnitude and timing of precipitation have a significant impact on the wet deposition rates. Second, the representation of aerosol-cloud interactions within the different models and resolutions can alter the number of dust aerosols that are activated and act as CCNs and INs. The explicit treatment of aerosol as ice nuclei is not included in the WRF-Chem version used in this study (Berg et al., 2015). Uncertainties of scavenging processes of aerosols within and below clouds impacts the deposition rates.

A better understanding of how orographically forced precipitation events are impacted in the presence of dust is crucial for the better understanding of wet removal processes. A study that quantifies the removal by convective and synoptic precipitation over mountain regions during dust events will give us a better understanding of the dominant processes and their uncertainties.

In summary, we have shown:

- An extreme dust deposition event occurred in April 2018, that is in the top 5% of dust transport events to the Alps during the snow season detected by satellite between 2002-2021 snow seasons.
- Dust for this event was transported to Col du Lautaret specifically from the northern portion of Africa, representing a filament of a larger dust transported event that transported a significant amount of dust farther east.
- This dust transport event occurred within a developing storm that resulted in significant precipitation (snow/rain) as it arrived in the Alps.
- Model predictions of dust deposition to snow have different spatial and temporal properties, with mainly under predicted wet deposition to the Col du Lautaret site.

- For this event, WRF-Chem model predicts that both wet (∼79.5%) and dry deposition (∼20.5%) contribute to total dust deposition. (wet deposition 84.5 % and dry deposition 15.5% at altitudes above 850 m over the Alps)
- Dry deposition is a key removal process at the western part of the French Alps at low altitudes, while wet deposition dominates over the complex higher altitude mountain terrain.
- Our specific WRF-Chem setup improved dust deposition predictions compared to CAMS, when evaluated against observations.
- The main differences in model predicted deposition are not co-located with the measurement site, but instead are located at lower elevations for dry deposition and co-located with improved predictions of precipitation (for D03) for wet deposition.
- Total dust deposition for this event increase in the Alps and decreases at Po Valley upon increasing model resolution (WRF-Chem D03).
- Deposition fluxes over the Alps are strongly dominated by the coarse size bins i.e particles with diameters over 0.9μm for CAMS and 1.25 μm for WRF-Chem during this event.

This study shows that WRF-Chem predicts the full lifecycle of dust from initial emissions, transport and processing in the atmosphere, and removal via wet and dry deposition but improvements in model dust emissions and aerosol scavenging is needed. For example, a better representation of dust emissions within WRF-Chem by improving soil moisture data from satellite retrievals could improve the dust particle mass distribution, thus impacting emissions, transport, and deposition processes. In addition, measurements of dry deposition velocities over the domain of interest could help us better estimate the emitted and transported dust and may help us improve the dry deposition parameterizations within the model. Furthermore, the explicit treatment of aerosol as ice nuclei could improve dust scavenging from clouds. This study also shows that CAMS predicts well dust concentration within the atmosphere but underestimates dust deposition fluxes for the simulated event at Col du Lautaret. The episodic nature of dust deposition can result to inter-annual fluctuations of seasonal snow melt rate and shortening of snow season. The accurate representation of dust deposition fluxes is important for quantifying these changes. The underestimation of dust deposition fluxes over glaciers and seasonal snow cover mountain regions can have a significant impact on projections of future climate change.

Table 1. WRF-Chem 4.1.0 setup.

Description	D01 (27×27 km)	D02 (9×9 km)	D03 (3×3 km)
Physics options and inputs			
Planet. bound. layer	YSU (Hong et al., 2006)	→	→
Surface layer	Revised MM5 Scheme (Jiménez et al., 2012)	→	→
Land surface	Noah-MP(Niu et al., 2011)	→	→
Microphysics	Morrison (Morrison et al., 2009)	→	→
SW radiation	Dudhia Scheme (Dudhia, 1989)	→	→
LW radiation	RRTM Longwave Scheme (Mlawer et al., 1997)	→	→
Cumulus param.	Kain-Fritsch - CuP(Berg et al., 2015)	→	See note[a]
Mountain Options	Not activated	Not activated	See note[b]
Physics initial cond.	ERA5 (Hersbach et al., 2020)	→	→
Physics bound. cond.	ERA5 (Hersbach et al., 2020)	D01	D02
Chemistry options and inputs			
Aerosol chem.	MOSAIC 8 bins (Zaveri et al., 2008) with VBS-2 SOA formation & aq. chem.	→	→
Gas-phase chemistry	SAPRC-99(Carter, 2000)	→	→
Chemical initial cond.	CAM-Chem (Buchholz et al., 2019)	→	→
Chemical bound. cond.	CAM-Chem (Buchholz et al., 2019)	D01	D02
Anthro. emiss.	CAMS (Granier et al., 2019)	→	→
Fire emiss.	FINN (Wiedinmyer et al., 2011)	→	→
Biogenic emiss.	MEGAN (Guenther et al., 2006)	→	→
Dust emiss.	GOCART (Chin et al., 2002)[c]	→	→

[a] a sensitivity run with this on also for D03 was completed

[b] slope effect on surface solar radiation, shadowing of neighbouring grid cells

[c] updated according to (Shao et al., 2011)

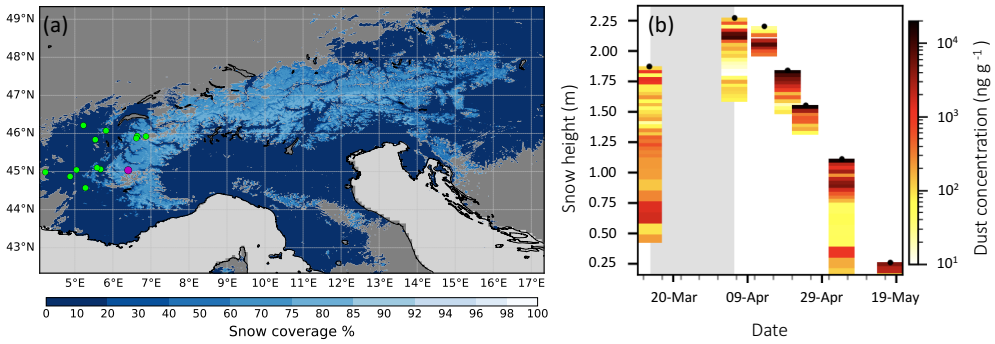

Figure 1. (a) Spatial extent of snow cover in the Alps on 22 March 2018 from MODIS/Terra. Magenta cycle presents Col du Lautaret site. Green circles show the location of ground PM10 measurement sites used in Figure 7. (b) Dust concentrations measured in snow pits at the Col du Lautaret during spring 2018 originally published in (Tuzet et al., 2019). Light gray shaded area corresponds to dust deposition events that occurred between 13 March and 4 April 2018. High dust concentration measurements are depicted with dark red color. Each black dot corresponds to a snowpit measurement. Snow height is given as height above ground level.

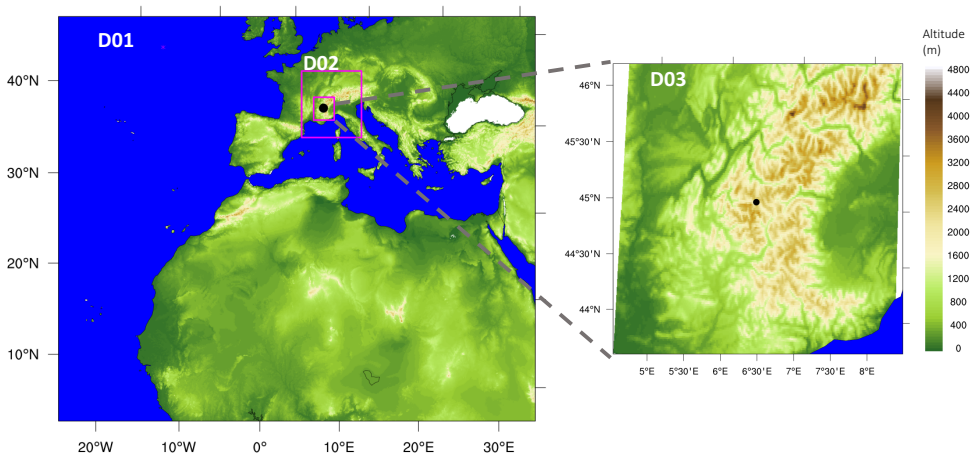

Figure 2. The WRF-Chem simulation domains (and associated horizontal model resolutions): D01 (27 km), D02 (9 km), and D03 (3 km, zoom in on right). The model topography (color bar) and domain boundaries (pink) are shown.

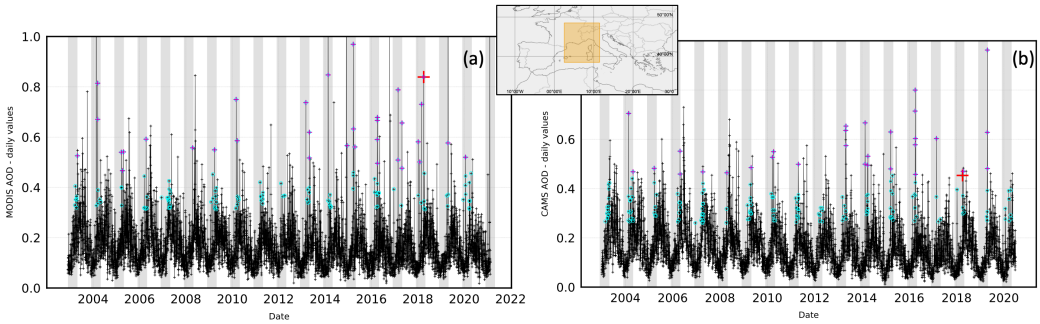

Figure 3. Time series of the spatial average over the box : 2.5°E, 38.5°N, 11.5°E, 48.5°N (inset pane) of daily mean AOD from MODIS Aqua (550 nm) (a) and CAMS reanalysis (b) for the period July 2002/2003 to February 2020/2021. Magenta and teal cycles present the 95 and 99 percentile of AOD during the snow season (December to April) accordingly. The Red Cross presents the simulated dust event in April 2018. Light gray shaded areas correspond to the snow season (December-April).

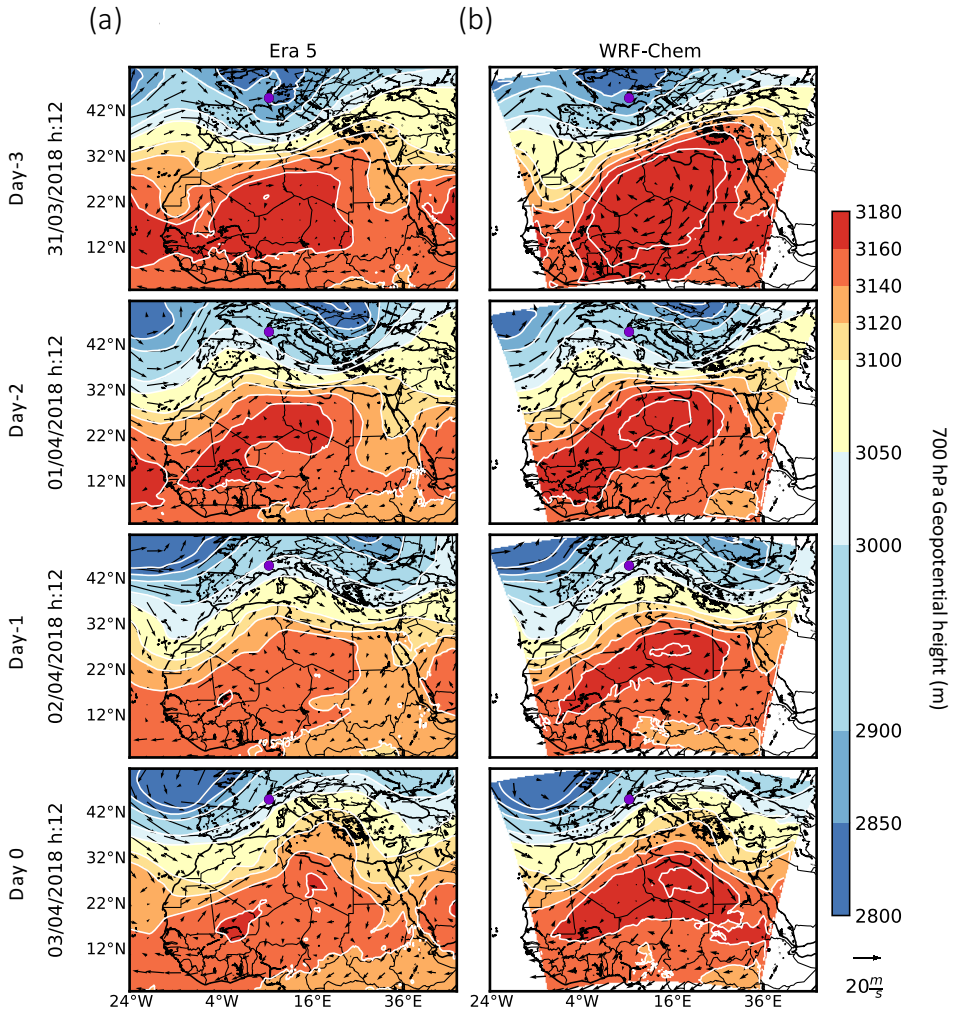

Figure 4. 700 hPa Geopotential height (contour) and wind speed (arrows) (a) from ERA5 (b) from WRF-Chem at 12:00 UTC from 31 March to 3 of April 2018.

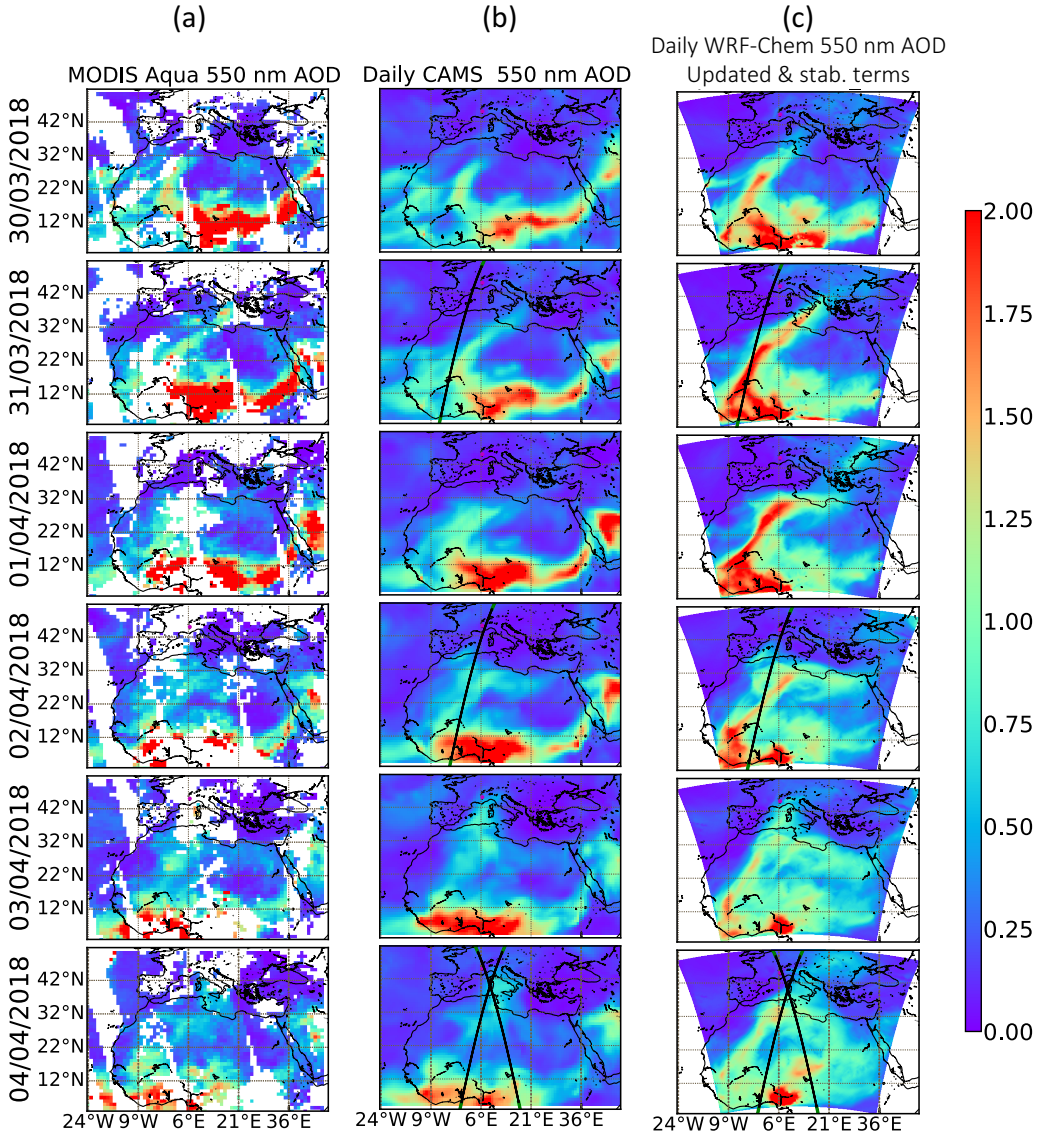

Figure 5. The 550 nm AOD from 30 March to 04 April 2018 from MODIS Aqua (a-f) compared to CAMS reanalysis (g-l) and WRF-Chem D01 simulated values (m-r) on the same days. CALIPSO overpasses are shown in black and green; the black portion of the overpass indicates the data used in Figure 5.

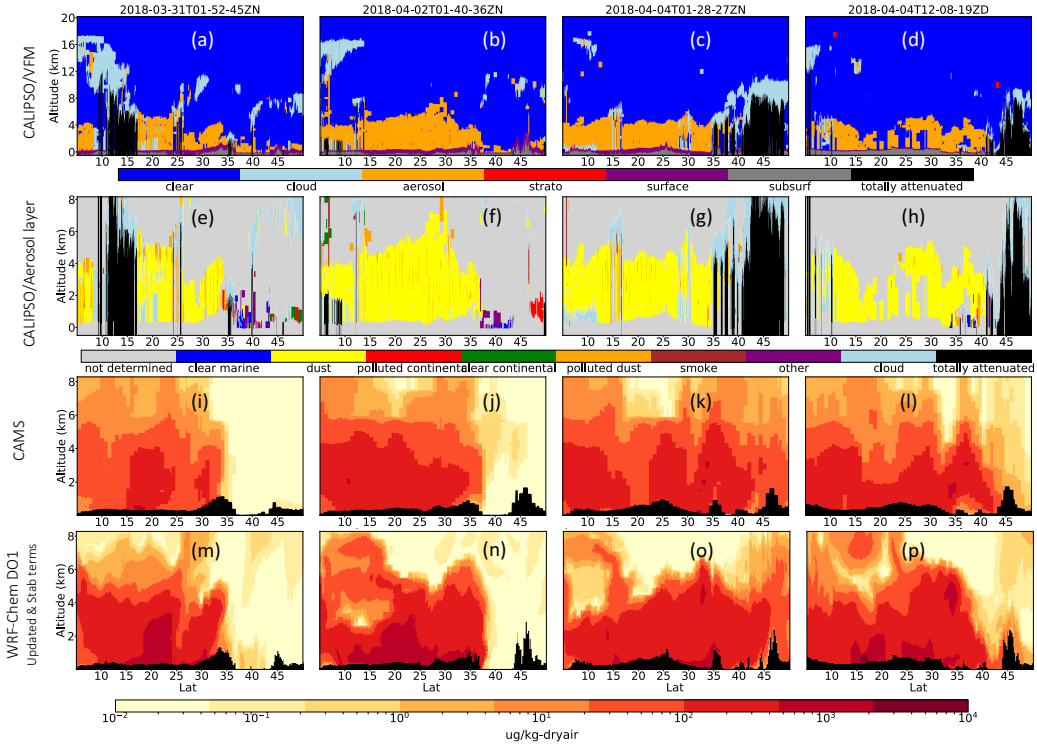

Figure 6. First row panels (a-d) show the Vertical feature mask (VFM) from the CALIPSO overpass on 31 March 2018 (01:52 UTC to 02:06 UTC), 2 April 2018 01:40 UTC to 01:54 UTC), 4 April 2018 (01:28 UTC to 01:42 UTC), 4 April 2018 (12:08 UTC to 12:21 UTC). Second row panels (e-h) show the vertical sub-types of aerosols, yellow color indicates dust. Third row panels (i - l)show the CAMS reanalysis and forth row panels show WRF-Chem model results of dust mixing ratio extracted along the overpasses.

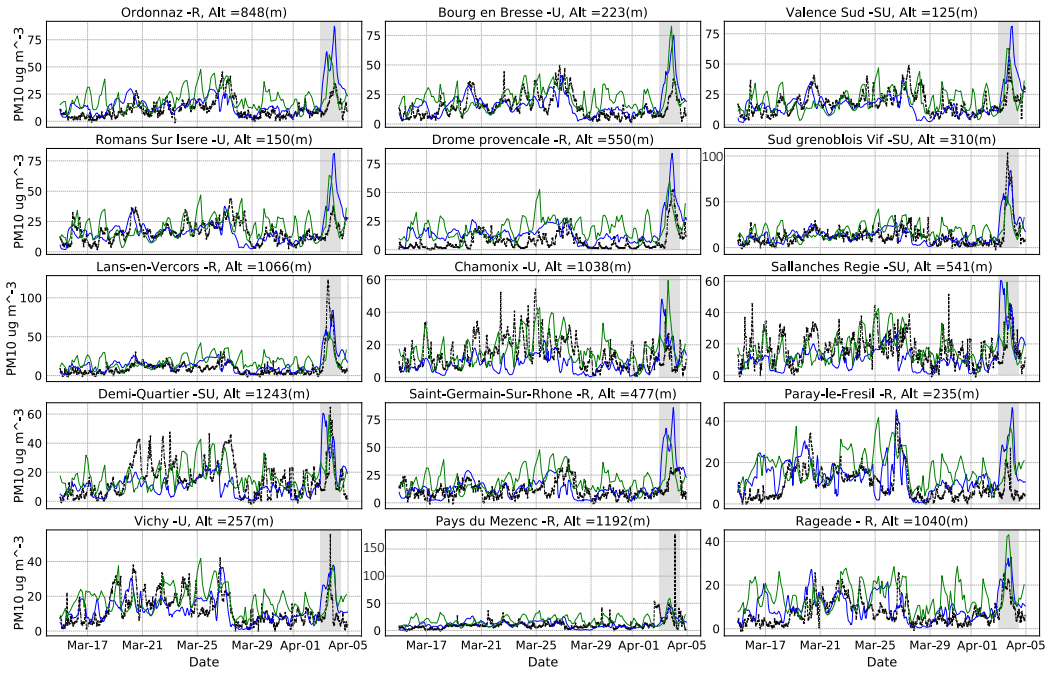

Figure 7. Hourly PM10 mass observations near the French Alps (black color) and the corresponding WRF-Chem D01 simulated values (blue color) and CAMS values (green color) for 15 March 2018 to 5 April 2018. Light gray shaded area corresponds to dust deposition event for the period 3 April and 4 April 12:00 UTC 2018.

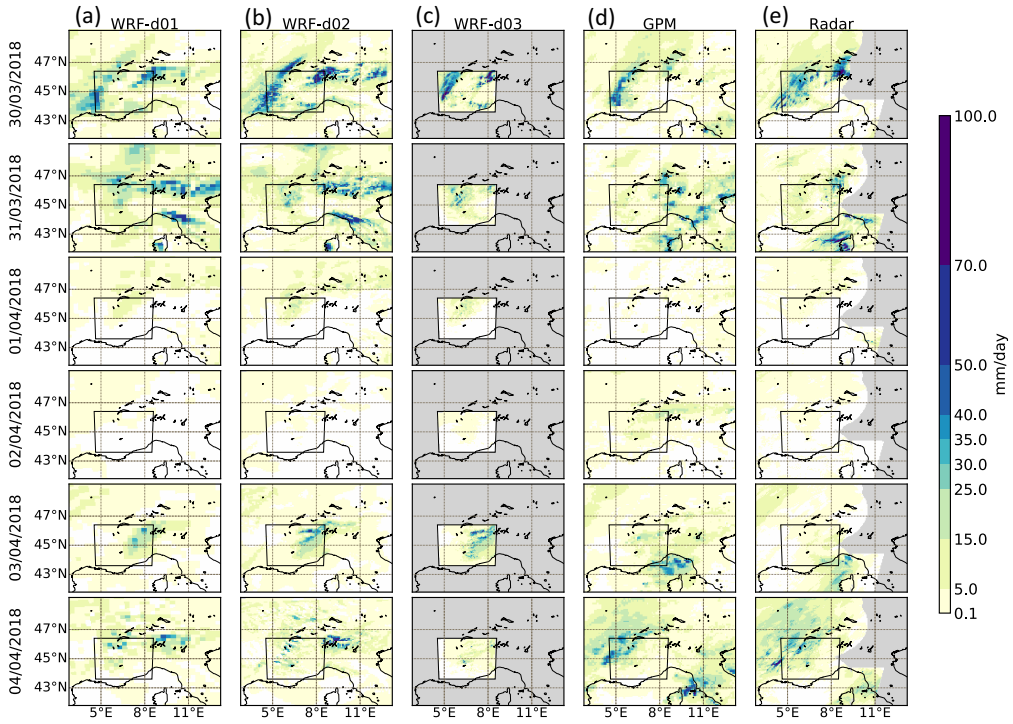

Figure 8. Spatial distribution of co-located WRF-D01 - (a), WRF-D02 - (b), WRF-D03 - (c), GPM - (d), Météo-France Mosaic Radar - (e), total daily precipitation from 30 March to 4 April. Grey color indicates no data; white color indicates daily precipitation less than 0.1 mm/day. The inner black box depicts the perimeter of WRF-D03.

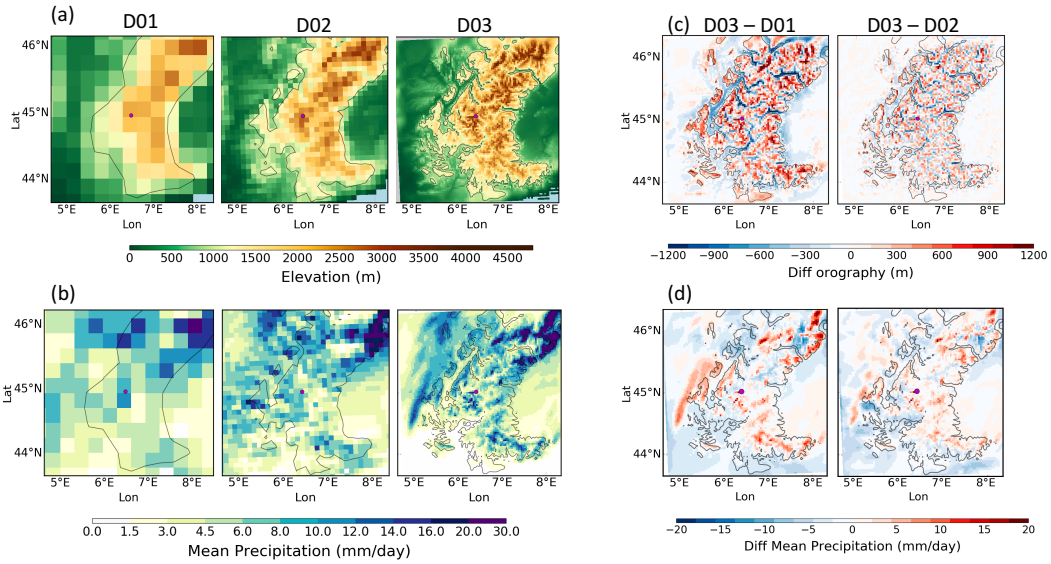

Figure 9. Orography (a) and accumulated predicted precipitation (b) from WRF-Chem at different resolutions during the event across the French Alps. Differences between the different resolutions/domains of orography and mean precipitation are shown at panels (c) and (d) accordingly. The black solid line represents the contour line at 1000 m altitude height. Purple dot depicts Col de Lautaret.

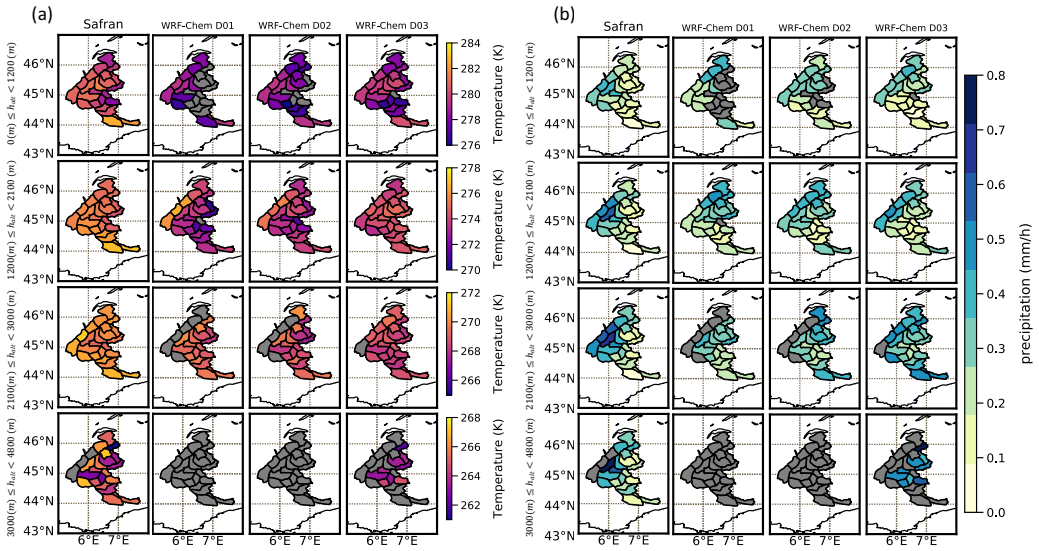

Figure 10. Spatial distribution of co-located binned SAFRAN (first column panels), WRF-D01 (second column panels), WRF-D02 (third column panels), WRF-D03 (fourth column panels), mean temperature - (a) , hourly precipitation (b) from 30 March to 3 April 2018. The first row represents data at altitudes (a.s.l.) below 1200 m, the second row above 1200 m and below 2100 m , the third row above 2100 m and below 3000 m and the fourth row 3000 m and above. Grey color indicates no data.

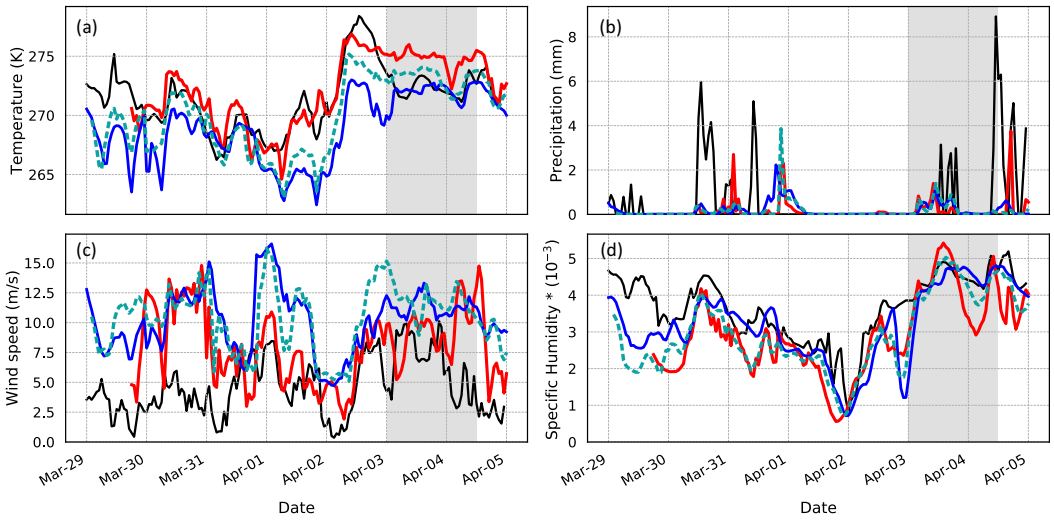

Figure 11. Plot of temperature at 2m height (a), 1h accumulated precipitation (b), and wind speed (c), specific humidity (d) measured during the 30 March and 4 April event at the Col du Lautaret site. WRF-Chem simulated values of D01, D02 , D03 are depicted by colors blue, teal and red accordingly. Measurement values are illustrated with black color. Light gray shaded area corresponds to dust deposition event for the period 3 April and 4 April 12:00 UTC 2018.

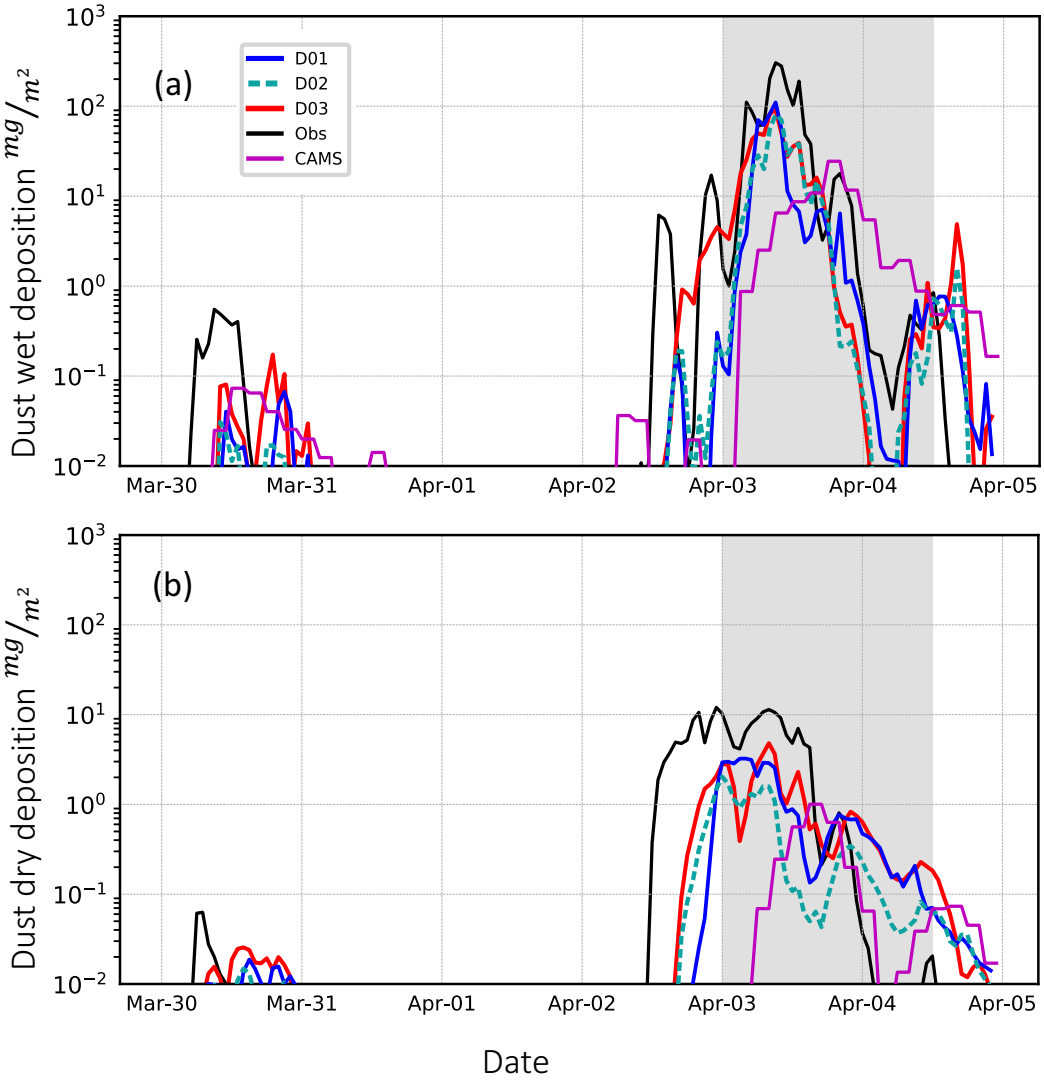

Figure 12. Model predicted 1h accumulated wet (a) and dry (b) deposition of dust at Col du Lautaret. WRF simulated values of D01, D02 , D03 are depicted by colors blue, teal and red accordingly and CAMS reanalysis values by magenta. Aladin simulated values "corrected" by observations are illustrated with black color.

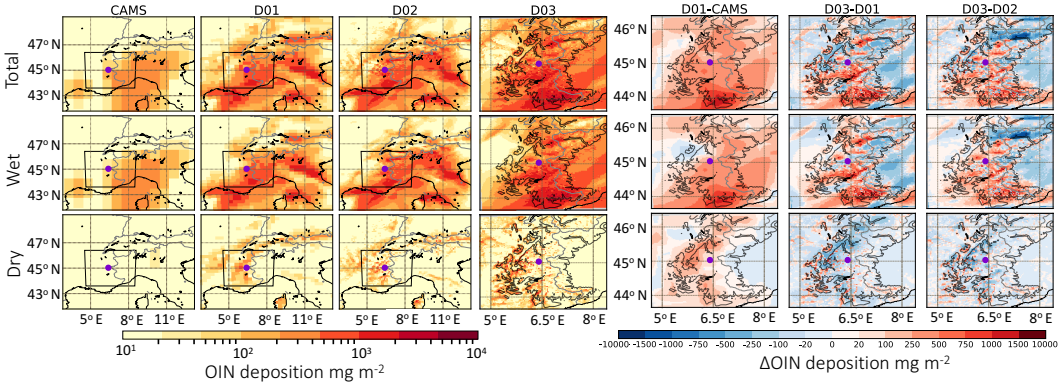

Figure 13. Accumulated dust from CAMS reanalysis and predicted OIN. Total (wet & dry) (first row panels) , wet (second row panels) and dry (third row panels) deposition across the Alps on 3 of April 2018. WRF-Chem D01 and CAMS values are depicted over the geographical limits of D02 in order to illustrate and compare the dust deposition rates over the Alpine region. CAMS values are shown on first column panels, WRF-Chem D01 are second column panels D02 are third column panels and D03 forth column panels. Differences between D01 and CAMS as well as between D03 and D01 and D03 and D02 are shown at the fifth, sixth and seventh column panels accordingly. The inner black box at the first (CAMS) and second (D01) and third (D02) column panels represents the geographical limits of D03. The black solid line represents the contour line at 1000 m altitude height. Purple dot depicts Col du Lautaret.

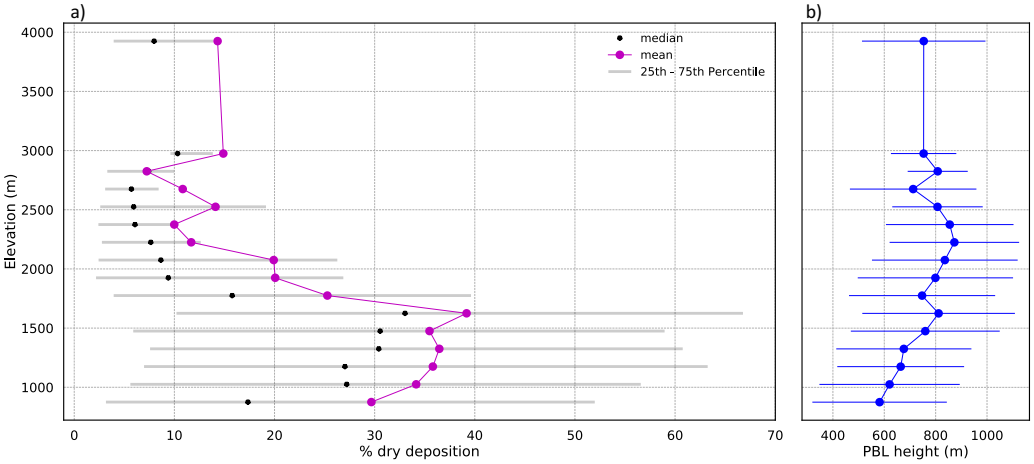

Figure 14. Altitude dependence of (a) the percentage dry to total modeled deposition; black asterisks represents the median and magenta dots the mean values, grey line depicts the 25th to 75th percentile intervals, (b) PBL height; blue line presents the standard deviation and shows the spatial variability in each elevation bin, from WRF-Chem D03 at the western French Alps (longitudes less than 6.5°E) on 3rd of April 2018. Deposition rates and PBL heights are binned at 150 m intervals from 800 to 3050 m, and the last bin includes the values above 3050 m.

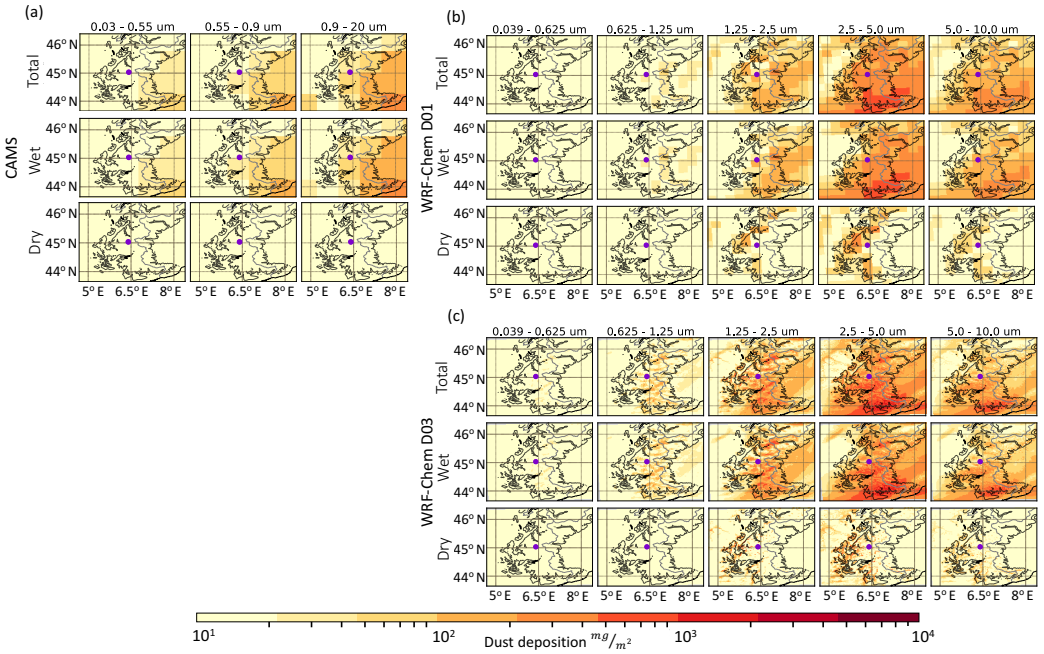

Figure 15. Accumulated dust from CAMS reanalysis and WRF-Chem OIN predicted total (wet & dry) (first row panels) , wet (second row panels) and dry (third row panels) deposition at different size bins across the Alps on 3 of April 2018. CAMS panel (a) and WRF-Chem D01 panel (b) and D03 panel (c) values are depicted over the geographical limits of WRF-Chem D03 in order to illustrate the dust deposition rates over the Alpine region. Size bin 0.039-0.625 μm includes the WRF-Chem D01 accumulated dust deposition rates from the first 4 size bins (0.039-0.078 μm, 0.078-0.156 μm, 0.156-0.312μm, 0.312-0.625 μm). The black solid line represents the contour line at 1000m altitude height. Purple dot depicts Col du Lautaret.

Acknowledgments

IGE and CNRM–CEN are part of Labex OSUG@2020 (investissement d'avenir – ANR10 LABX56). This work was performed using HPC resources from GENCI-ID-RIS (Grant A007017141) and the IPSL mesoscale computing center (CICLAD: Calcul Intensif pour le CLimat, l'Atmosphère et la Dynamique). This study was supported by the Ecole Doctorale Terre Univers Environnement of Grenoble and part of it by Early Career Scientist Assembly (ECSA) FY2020 National Center for Atmospheric Research/Research Applications Laboratory (NCAR/RAL) sponsored by the National Science Foundation (NSF). This work was partly supported by Lautaret Garden – UMS 3370 (Univ. Grenoble Alpes, CNRS,SAJF, 38000 Grenoble, France), a member of AnaEE France (ANR-11-INBS- 0001 AnaEE-Services, Investissements d'Avenir frame) and of the eLTER European network (Univ. Grenoble Alpes, CNRS, LTSER Zone Atelier Alpes, 38000 Grenoble, France) and by ANR grant EBONI (ANR-16-CE01-0006). Marie Dumont has received funding from the European Research Council (ERC) under the European Union's Horizon 2020 research and innovation programme (grant agreement No 949516, IVORI). We acknowledge Institute of Environmental Geosciences (IGE) for administrative support. We acknowledge use of the WRF-Chem pre-processor tools provided by the Atmospheric Chemistry Observations and Modeling Lab (ACOM) of NCAR. We acknowledge NCAR ACOM for providing the WRF-Chem chemical boundary conditions used in this study. We acknowledge Meteo France for providing SAFRAN reanalysis data used in this study. We acknowledge the NASA/Goddard Space Flight Center's PMM Science

Team and PPS, which develop and compute the Integrated Multi-satellitE Retrievals as a contribution to GPM, and archived at the NASA GES DISC. We acknowledge the Emissions of atmospheric Compounds and Compilation of Ancillary Data (ECCAD) for providing anthropogenic emissions used in this study. We thank the CAMS development and support teams at ECMWF for providing dust deposition rates used in this study. We thank B. Boudevillain and F.Tuzet for supporting this work by providing helpful information for observation data used in this study.

Data Availability Statement

Col du Lautaret in situ measurements are available at https://doi.org/10.18709/perscido.2020.09.ds330. CAMS deposition fluxes data are available by contacting M.Parrington and/or J.Flemming by email (Mark.Parrington@ecmwf.int, Johannes.Flemming@ecmwf.int). The radar rainfall mosaic data is available from https://radarsmf.aeris-data.fr/. The code used for this study is available on Zenodo https://doi.org/10.5281/zenodo.5221694 .

References

Benedetti, A., & Fisher, M. (2007). Background error statistics for aerosols. *Quarterly Journal of the Royal Meteorological Society: A journal of the atmospheric sciences, applied meteorology and physical oceanography*, *133*(623), 391–405.

Benedetti, A., Giuseppe, F. D., Jones, L., Peuch, V.-H., Rémy, S., & Zhang, X. (2019). The value of satellite observations in the analysis and short-range prediction of asian dust. *Atmospheric Chemistry and Physics*, *19*(2), 987–998.

Benedetti, A., Morcrette, J., Boucher, O., Dethof, A., Engelen, R., Fisher, M., ... Kinne (2009). the gems-aer team: Aerosol analysis and forecast in the ecmwf integrated forecast system. part ii: Data assimilation. *J. Geophys. Res*, *114*, D13205.

Berg, L. K., Shrivastava, M., Easter, R. C., Fast, J. D., Chapman, E. G., Liu, Y., & Ferrare, R. (2015). A new wrf-chem treatment for studying regional-scale impacts of cloud processes on aerosol and trace gases in parameterized cumuli. *Geoscientific Model Development (Online)*, *8*(2).

Bessagnet, B., Menut, L., Colette, A., Couvidat, F., Dan, M., Mailler, S., ... Rouïl, L. (2017). An evaluation of the chimere chemistry transport model to simulate dust outbreaks across the northern hemisphere in march 2014. *Atmosphere*, *8*(12), 251.

Buchholz, R., Emmons, L., & Tilmes, S. (2019). *The cesm2 development team: Cesm2. 1/cam-chem instantaneous output for boundary conditions, ucar/ncar–atmospheric chemistry observations and modeling laboratory, subset used 3° - 52° n and 24.75° w - 48° e., accessed 16 jul 2019.*

Carter, W. P. (2000). Documentation of the saprc-99 chemical mechanism for voc reactivity assessment. *Contract*, *92*(329), 95–308.

Chiapello, I., Bergametti, G., Chatenet, B., Bousquet, P., Dulac, F., & Soares, E. S. (1997). Origins of african dust transported over the northeastern tropical atlantic. *Journal of Geophysical Research: Atmospheres*, *102*(D12), 13701–13709.

Chin, M., Ginoux, P., Kinne, S., Torres, O., Holben, B. N., Duncan, B. N., ... Nakajima, T. (2002). Tropospheric aerosol optical thickness from the gocart model and comparisons with satellite and sun photometer measurements. *Journal of the atmospheric sciences*, *59*(3), 461–483.

Das, S., Giorgi, F., & Giuliani, G. (2020). Investigating the relative responses of regional monsoon dynamics to snow darkening and direct radiative effects of dust and carbonaceous aerosols over the indian subcontinent. *Climate Dynamics*, *55*, 1011–1030.

Deems, J. S., Painter, T. H., Barsugli, J. J., Belnap, J., & Udall, B. (2013). Combined impacts of current and future dust deposition and regional warming

on colorado river basin snow dynamics and hydrology. *Hydrology and Earth System Sciences*, *17*(11), 4401–4413.

Di Mauro, B., Garzonio, R., Rossini, M., Filippa, G., Pogliotti, P., Galvagno, M., ... others (2019). Saharan dust events in the european alps: role in snowmelt and geochemical characterization. *The Cryosphere*, *13*(4), 1147–1165.

Dudhia, J. (1989). Numerical study of convection observed during the winter monsoon experiment using a mesoscale two-dimensional model. *Journal of Atmospheric Sciences*, *46*(20), 3077–3107.

Durand, Y., Giraud, G., Laternser, M., Etchevers, P., Mérindol, L., & Lesaffre, B. (2009). Reanalysis of 47 years of climate in the french alps (1958–2005): climatology and trends for snow cover. *Journal of applied meteorology and climatology*, *48*(12), 2487–2512.

Easter, R. C., Ghan, S. J., Zhang, Y., Saylor, R. D., Chapman, E. G., Laulainen, N. S., ... Zaveri, R. A. (2004). Mirage: Model description and evaluation of aerosols and trace gases. *Journal of Geophysical Research: Atmospheres*, *109*(D20).

ECMWF. (2021). *Reanalysis*. `https://www.ecmwf.int/en/about/media-centre/focus/2020/fact-sheet-reanalysis`. (Online; accessed 9-June-2021)

Fast, J., Craven, J., Metcalf, A., & Seinfeld, J. (2014). Modeling regional aerosol and aerosol precursor variability over california and its sensitivity to emissions and long-range transport during the 2010 calnex and cares campaigns. *Atmospheric Chemistry and Physics*, *14*(18), 10013–10060.

Fast, J. D., Gustafson Jr, W. I., Easter, R. C., Zaveri, R. A., Barnard, J. C., Chapman, E. G., ... Peckham, S. E. (2006). Evolution of ozone, particulates, and aerosol direct radiative forcing in the vicinity of houston using a fully coupled meteorology-chemistry-aerosol model. *Journal of Geophysical Research: Atmospheres*, *111*(D21).

Flanner, M., Liu, X., Zhou, C., Penner, J. E., & Jiao, C. (2012). Enhanced solar energy absorption by internally-mixed black carbon in snow grains. *Atmospheric Chemistry and Physics*, *12*(10), 4699.

Flanner, M. G., Zender, C. S., Randerson, J. T., & Rasch, P. J. (2007). Present-day climate forcing and response from black carbon in snow. *Journal of Geophysical Research: Atmospheres*, *112*(D11).

García-Díez, M., Fernández, J., Fita, L., & Yagüe, C. (2013). Seasonal dependence of wrf model biases and sensitivity to pbl schemes over europe. *Quarterly Journal of the Royal Meteorological Society*, *139*(671), 501–514.

Ginoux, P., Chin, M., Tegen, I., Prospero, J. M., Holben, B., Dubovik, O., & Lin, S.-J. (2001). Sources and distributions of dust aerosols simulated with the gocart model. *Journal of Geophysical Research: Atmospheres*, *106*(D17), 20255–20273.

Goudie, A., & Middleton, N. (2001). Saharan dust storms: nature and consequences. *Earth-science reviews*, *56*(1-4), 179–204.

Granier, C., Darras, S., Denier van der Gon, H., Doubalova, J., Elguindi, N., Galle, B., ... Liousse (2019). The copernicus atmosphere monitoring service global and regional emissions. *Reading, United Kingdom: Copernicus Atmosphere Monitoring Service. https://doi. org/10.24380/d0bn-kx16*.

Grell, G. A., Peckham, S. E., Schmitz, R., McKeen, S. A., Frost, G., Skamarock, W. C., & Eder, B. (2005). Fully coupled "online" chemistry within the wrf model. *Atmospheric Environment*, *39*(37), 6957–6975.

Guenther, A., Karl, T., Harley, P., Wiedinmyer, C., Palmer, P. I., & Geron, C. (2006). Estimates of global terrestrial isoprene emissions using megan (model of emissions of gases and aerosols from nature). *Atmospheric Chemistry and Physics*, *6*(11), 3181–3210.

Hansen, J., & Nazarenko, L. (2004). Soot climate forcing via snow and ice albedos. *Proceedings of the National Academy of Sciences*, *101*(2), 423–428.

Hansen, J., Sato, M., & Ruedy, R. (1997). Radiative forcing and climate response. *Journal of Geophysical Research: Atmospheres*, *102*(D6), 6831–6864.

Haywood, J., & Boucher, O. (2000). Estimates of the direct and indirect radiative forcing due to tropospheric aerosols: A review. *Reviews of geophysics*, *38*(4), 513–543.

Hersbach, H., Bell, B., Berrisford, P., Hirahara, S., Horányi, A., Muñoz-Sabater, J., ... Thépaut, J.-N. (2020). The era5 global reanalysis. *Quarterly Journal of the Royal Meteorological Society*, *146*(730), 1999-2049. Retrieved from https://rmets.onlinelibrary.wiley.com/doi/abs/10.1002/qj.3803 doi: https://doi.org/10.1002/qj.3803

Hock, R., Rasul, G., Adler, C., Cáceres, B., Gruber, S., Hirabayashi, Y., ... Milner (2019). *High mountain areas: In: Ipcc special report on the ocean and cryosphere in a changing climate.*

Hong, S.-Y., Noh, Y., & Dudhia, J. (2006). A new vertical diffusion package with an explicit treatment of entrainment processes. *Monthly weather review*, *134*(9), 2318–2341.

Huffman, G., Stocker, E., Bolvin, D., Nelkin, E., & Tan, J. (2019). Gpm imerg final precipitation l3 1 day 0.1 degree x 0.1 degree v06, edited by andrey savtchenko, greenbelt, md, goddard earth sciences data and information services center (ges disc), accessed 27 september 2019. *doi. org/10.5067/GPM/IMERG DF/DAY/06*.

Huneeus, N., Schulz, M., Balkanski, Y., Griesfeller, J., Prospero, J., Kinne, S., ... others (2011). Global dust model intercomparison in aerocom phase i. *Atmospheric Chemistry and Physics*, *11*(15), 7781–7816.

Inness, A., Ades, M., Agustí-Panareda, A., Barré, J., Benedictow, A., Blechschmidt, A.-M., ... Suttie, M. (2019). The cams reanalysis of atmospheric composition. *Atmospheric Chemistry and Physics*, *19*(6), 3515–3556. Retrieved from https://acp.copernicus.org/articles/19/3515/2019/ doi: 10.5194/acp-19-3515-2019

Jiménez, P. A., & Dudhia, J. (2013). On the ability of the wrf model to reproduce the surface wind direction over complex terrain. *Journal of Applied Meteorology and Climatology*, *52*(7), 1610–1617.

Jiménez, P. A., Dudhia, J., González-Rouco, J. F., Navarro, J., Montávez, J. P., & García-Bustamante, E. (2012). A revised scheme for the wrf surface layer formulation. *Monthly Weather Review*, *140*(3), 898–918.

Karki, R., ul Hasson, S., Gerlitz, L., Schickhoff, U., Scholten, T., & Böhner, J. (2017). Quantifying the added value of convection-permitting climate simulations in complex terrain: a systematic evaluation of wrf over the himalayas. *Earth System Dynamics*, *8*(3), 507–528. Retrieved from https://esd.copernicus.org/articles/8/507/2017/ doi: 10.5194/esd-8-507-2017

Kok, J. F., Adebiyi, A. A., Albani, S., Balkanski, Y., Checa-Garcia, R., Chin, M., ... Wan, J. S. (2021). Contribution of the world's main dust source regions to the global cycle of desert dust. *Atmospheric Chemistry and Physics*, *21*(10), 8169–8193. Retrieved from https://acp.copernicus.org/articles/21/8169/2021/ doi: 10.5194/acp-21-8169-2021

Kok, J. F., Parteli, E. J., Michaels, T. I., & Karam, D. B. (2012). The physics of wind-blown sand and dust. *Reports on progress in Physics*, *75*(10), 106901.

Kumar, R., Naja, M., Pfister, G., Barth, M., & Brasseur, G. (2012). Simulations over south asia using the weather research and forecasting model with chemistry (wrf-chem): set-up and meteorological evaluation. *Geoscientific Model Development*, *5*(2), 321–343.

Lau, W. K. M., & Kim, K.-M. (2018). Impact of snow darkening by deposition of light-absorbing aerosols on snow cover in the himalayas–tibetan plateau and influence on the asian summer monsoon: A possible mechanism for the blanford hypothesis. *Atmosphere*, *9*(11). Retrieved from

https://www.mdpi.com/2073-4433/9/11/438 doi: 10.3390/atmos9110438

Levy, R. C., Mattoo, S., Sawyer, V., Shi, Y., Colarco, P. R., Lyapustin, A. I., ... Remer, L. A. (2018). Exploring systematic offsets between aerosol products from the two modis sensors. *Atmospheric measurement techniques*, *11*(7), 4073–4092.

Mahowald, N., Albani, S., Kok, J. F., Engelstaeder, S., Scanza, R., Ward, D. S., & Flanner, M. G. (2014). The size distribution of desert dust aerosols and its impact on the earth system. *Aeolian Research*, *15*, 53–71.

Marelle, L., Raut, J.-C., Law, K. S., Berg, L. K., Fast, J. D., Easter, R. C., ... Thomas, J. L. (2017). Improvements to the wrf-chem 3.5. 1 model for quasi-hemispheric simulations of aerosols and ozone in the arctic. *Geoscientific Model Development*, *10*(10), 3661–3677.

Meng, X., Lyu, S., Zhang, T., Zhao, L., Li, Z., Han, B., ... Wen, L. (2018, apr). Simulated cold bias being improved by using MODIS time-varying albedo in the tibetan plateau in WRF model. *Environmental Research Letters*, *13*(4), 044028. Retrieved from https://doi.org/10.1088/1748-9326/aab44a doi: 10.1088/1748-9326/aab44a

Meteo France. (2021). *Weather regimes.* http://seasonal.meteo.fr/content/suivi-clim-regimes-quot?language=en. (Online; accessed 9-June-2021)

Miguez-Macho, G., Stenchikov, G. L., & Robock, A. (2004). Spectral nudging to eliminate the effects of domain position and geometry in regional climate model simulations. *Journal of Geophysical Research: Atmospheres*, *109*(D13).

Mlawer, E. J., Taubman, S. J., Brown, P. D., Iacono, M. J., & Clough, S. A. (1997). Radiative transfer for inhomogeneous atmospheres: Rrtm, a validated correlated-k model for the longwave. *Journal of Geophysical Research: Atmospheres*, *102*(D14), 16663–16682.

Morcrette, J.-J., Boucher, O., Jones, L., Salmond, D., Bechtold, P., Beljaars, A., ... Untch, A. (2009). Aerosol analysis and forecast in the european centre for medium-range weather forecasts integrated forecast system: Forward modeling. *Journal of Geophysical Research: Atmospheres*, *114*(D6). Retrieved from https://agupubs.onlinelibrary.wiley.com/doi/abs/10.1029/2008JD011235 doi: https://doi.org/10.1029/2008JD011235

Morrison, H., Thompson, G., & Tatarskii, V. (2009). Impact of cloud microphysics on the development of trailing stratiform precipitation in a simulated squall line: Comparison of one-and two-moment schemes. *Monthly weather review*, *137*(3), 991–1007.

Niu, G.-Y., Yang, Z.-L., Mitchell, K. E., Chen, F., Ek, M. B., Barlage, M., ... Xia, Y. (2011). The community noah land surface model with multiparameterization options (noah-mp): 1. model description and evaluation with local-scale measurements. *Journal of Geophysical Research: Atmospheres*, *116*(D12). Retrieved from https://agupubs.onlinelibrary.wiley.com/doi/abs/10.1029/2010JD015139 doi: https://doi.org/10.1029/2010JD015139

Omar, A. H., Winker, D. M., Vaughan, M. A., Hu, Y., Trepte, C. R., Ferrare, R. A., ... Liu, Z. (2009). The calipso automated aerosol classification and lidar ratio selection algorithm. *Journal of Atmospheric and Oceanic Technology*, *26*(10), 1994 - 2014. Retrieved from https://journals.ametsoc.org/view/journals/atot/26/10/2009jtecha1231_1.xml doi: 10.1175/2009JTECHA1231.1

Painter, T. H., Barrett, A. P., Landry, C. C., Neff, J. C., Cassidy, M. P., Lawrence, C. R., ... Farmer, G. L. (2007). Impact of disturbed desert soils on duration of mountain snow cover. *Geophysical Research Letters*, *34*(12).

Painter, T. H., Bryant, A. C., & Skiles, S. M. (2012). Radiative forcing by light absorbing impurities in snow from modis surface reflectance data. *Geophysical Research Letters*, *39*(17).

Painter, T. H., Seidel, F. C., Bryant, A. C., McKenzie Skiles, S., & Rittger, K.

(2013). Imaging spectroscopy of albedo and radiative forcing by light-absorbing impurities in mountain snow. *Journal of Geophysical Research: Atmospheres*, *118*(17), 9511–9523.

Platnick, S., King, M. D., Meyer, K. G., Wind, G., Amarasinghe, N., Marchant, B., ... RIEDI (2015). Modis cloud optical properties: User guide for the collection 6 level-2 mod06/myd06 product and associated level-3 datasets. *Version*, *1*, 145.

Prospero, J. M., Delany, A. C., Delany, A. C., & Carlson, T. N. (2021). The discovery of african dust transport to the western hemisphere and the saharan air layer: A history. *Bulletin of the American Meteorological Society*, *102*(6), E1239 - E1260. Retrieved from `https://journals.ametsoc.org/view/journals/bams/102/6/BAMS-D-19-0309.1.xml` doi: 10.1175/BAMS-D-19-0309.1

Pruppacher, R., & Klett, J. (1997). Microphysics of clouds and precipitation , vol 18 kluwer academic publishers. *Atmospheric and Oceanographic Sciences Library*.

Rahimi, S., Liu, X., Zhao, C., Lu, Z., & Lebo, Z. J. (2020). Examining the atmospheric radiative and snow-darkening effects of black carbon and dust across the rocky mountains of the united states using wrf-chem. *Atmospheric Chemistry and Physics*, *20*(18), 10911–10935.

Regayre, L. A., Johnson, J. S., Yoshioka, M., Pringle, K. J., Sexton, D. M., Booth, B. B., ... Carslaw, K. S. (2018). Aerosol and physical atmosphere model parameters are both important sources of uncertainty in aerosol erf. *Atmospheric Chemistry and Physics*, *18*(13), 9975–10006.

Reynolds, R. L., Goldstein, H. L., Moskowitz, B. M., Bryant, A. C., Skiles, S. M., Kokaly, R. F., ... Painter, T. H. (2014). Composition of dust deposited to snow cover in the wasatch range (utah, usa): Controls on radiative properties of snow cover and comparison to some dust-source sediments. *Aeolian Research*, *15*, 73-90. Retrieved from `https://www.sciencedirect.com/science/article/pii/S1875963713000682` doi: https://doi.org/10.1016/j.aeolia.2013.08.001

Riggs, G. A., Hall, D. K., & Román, M. O. (2015). Modis snow products collection 6 user guide. *National Snow and Ice Data Center: Boulder, CO, USA*, 66.

Rotunno, R., & Houze, R. A. (2007). Lessons on orographic precipitation from the mesoscale alpine programme. *Quarterly Journal of the Royal Meteorological Society: A journal of the atmospheric sciences, applied meteorology and physical oceanography*, *133*(625), 811–830.

Salvador, P., Alonso-Pérez, S., Pey, J., Artíñano, B., De Bustos, J., Alastuey, A., & Querol, X. (2014). African dust outbreaks over the western mediterranean basin: 11-year characterization of atmospheric circulation patterns and dust source areas. *Atmospheric Chemistry and Physics*, *14*(13), 6759–6775.

Sarangi, C., Qian, Y., Rittger, K., Leung, L. R., Chand, D., Bormann, K. J., & Painter, T. H. (2020). Dust dominates high-altitude snow darkening and melt over high-mountain asia. *Nature Climate Change*, *10*(11), 1045–1051.

Seinfeld, J. H., & Pandis, S. N. (2016). *Atmospheric chemistry and physics: from air pollution to climate change*. John Wiley & Sons.

Shao, Y., Wyrwoll, K.-H., Chappell, A., Huang, J., Lin, Z., McTainsh, G. H., ... Yoon, S. (2011). Dust cycle: An emerging core theme in earth system science. *Aeolian Research*, *2*(4), 181–204.

Skamarock, W. C., & Klemp, J. B. (2008). A time-split nonhydrostatic atmospheric model for weather research and forecasting applications. *Journal of computational physics*, *227*(7), 3465–3485.

Skiles, S. M., Flanner, M., Cook, J. M., Dumont, M., & Painter, T. H. (2018). Radiative forcing by light-absorbing particles in snow. *Nature Climate Change*, *8*(11), 964–971.

Sodemann, H., Palmer, A., Schwierz, C., Schwikowski, M., & Wernli, H. (2006). The

transport history of two saharan dust events archived in an alpine ice core. *Atmospheric Chemistry and Physics*, *6*(3), 667–688.

Stocker, T. (2014). *Climate change 2013: the physical science basis: Working group i contribution to the fifth assessment report of the intergovernmental panel on climate change*. Cambridge university press.

Tuzet, F., Dumont, M., Arnaud, L., Voisin, D., Lamare, M., Larue, F., ... Picard, G. (2019). Influence of light-absorbing particles on snow spectral irradiance profiles. *Cryosphere*, *13*(8).

Tuzet, F., Dumont, M., Lafaysse, M., Picard, G., Laurent, A., Voisin, D., ... Morin, S. (2017). A multilayer physically based snowpack model simulating direct and indirect radiative impacts of light-absorbing impurities in snow. *The Cryosphere*, *11*(6), 2633.

Tuzet, F., Dumont, M., Picard, G., Lamare, M., Voisin, D., Nabat, P., ... Arnaud, L. (2020). Quantification of the radiative impact of light-absorbing particles during two contrasted snow seasons at col du lautaret (2058 m asl, french alps). *The Cryosphere*, *14*(12), 4553–4579.

Usha, K., Nair, V. S., & Babu, S. S. (2021). Effect of aerosol-induced snow darkening on the direct radiative effect of aerosols over the himalayan region. *Environmental Research Letters*, *16*(6), 064004.

Vionnet, V., Brun, E., Morin, S., Boone, A., Faroux, S., Le Moigne, P., ... Willemet, J.-M. (2012). The detailed snowpack scheme crocus and its implementation in surfex v7.2. *Geoscientific Model Development*, *5*(3), 773–791. Retrieved from `https://gmd.copernicus.org/articles/5/773/2012/` doi: 10.5194/gmd-5-773-2012

Wagenbach, D., & Geis, K. (1989). The mineral dust record in a high altitude alpine glacier (colle gnifetti, swiss alps).

Warren, S. G., & Wiscombe, W. J. (1980). A model for the spectral albedo of snow. ii: Snow containing atmospheric aerosols. *Journal of the Atmospheric Sciences*, *37*(12), 2734–2745.

Wesely, M. (1989). Parameterization of surface resistances to gaseous dry deposition in regional-scale numerical models. *Atmospheric Environment (1967)*, *23*(6), 1293–1304.

Wiedinmyer, C., Akagi, S., Yokelson, R. J., Emmons, L., Al-Saadi, J., Orlando, J., & Soja, A. (2011). The fire inventory from ncar (finn): A high resolution global model to estimate the emissions from open burning. *Geoscientific Model Development*, *4*(3), 625.

Yu, N., Gaussiat, N., & Tabary, P. (2018). Polarimetric x-band weather radars for quantitative precipitation estimation in mountainous regions. *Quarterly Journal of the Royal Meteorological Society*, *144*(717), 2603–2619.

Zaveri, R. A., Easter, R. C., Fast, J. D., & Peters, L. K. (2008). Model for simulating aerosol interactions and chemistry (mosaic). *Journal of Geophysical Research: Atmospheres*, *113*(D13).